


# Planform architecture, meander evolution and grain-size variability of a deltaic channel belt in the Rhine-Meuse delta, The Netherlands

TIMOTHEUS G. WINKELS , ESTHER STOUTHAMER and KIM M. COHEN  
Utrecht University Faculty of Geosciences – Physical Geography, Heidelberglaan 8, 3584 CS, Utrecht,  
The Netherlands (E-mail: t.g.winkels@uu.nl)

Associate Editor – Massimiliano Ghinassi

## ABSTRACT

In the unconstrained, low gradient setting of major delta plains, individual meander belts tend to function for relatively short periods of time due to repeated channel avulsion. Their short lifetime makes ‘deltaic’ channel belts suitable to study the products of steady meander evolution as the deposits and internal architectural elements preserved are often without complications of repeated bend cutoffs. This study investigated how sedimentary characteristics as preserved from subsequent stages of activity differ within the Stuivenberg channel belt. The Stuivenberg channel belt is a long-studied example in the Holocene Rhine-Meuse delta, The Netherlands, for which the meander evolution, i.e. geometry and dimensions through initiation, main activity and abandonment stages and durations of activity involved, was reconstructed. Mapping of the channel belt started from established coring based and LiDAR-aided methods. Explorative approaches were used to assess active channel width at the onset of abandonment, and to reconstruct meander positions during earlier stages. The migration history of five consecutive meanders is revealed from convex and concave ridge-and-swale scrolls. Analysis identifies them to be the product of translation, expansion and rotation trajectories during a period of 800 years. Grain-size composition throughout the sand body is interpreted given these positional contexts, with special attention to local coarsening of upper point bar facies in deltaic meander belts. The findings emphasize: (i) the need to separate abandonment stage from main activity stage when analysing three-dimensional channel belt architectures; and (ii) the influence of meander evolution on lithological characteristics of initial stage versus mature stage parts of deltaic channel belt sands.

**Keywords** Channel abandonment, channel belt sands, concave accretion zones, fluvial sedimentology, meander migration.

## INTRODUCTION

Classic sedimentological studies that described and characterized meandering river deposits (e.g. Fenneman, 1906; Leopold & Wolman, 1957; Allen, 1965) portray channel belts to consist of point-bar elements mostly. However, subsequent work has identified other brands of internal

architectural elements, which can compose a substantial part of the point bar complex, establishing that meandering river sand body architectures are more diverse (e.g. Miall, 1991; Jordan & Pryor, 1992; Aigner *et al.*, 1999; Toonen *et al.*, 2012; Colombera *et al.*, 2013). When describing the meandering channel belt architecture in planform, most studies aim to identify

and map distinct lithological units, attributing these to some mode of past channel shape shifting (mainly meander-bend migration dynamics – e.g. Nanson & Page, 1983; Smith *et al.*, 2009; Ielpi & Ghinassi, 2014; Russell *et al.*, 2019, or channel cut-off and abandonment dynamics – e.g. Fisk, 1947; Toonen *et al.*, 2012). Meander-bend migration morphology as studied through aerial photographs, LiDAR data or satellite imagery, in many cases reveals both concave and convex accretion zones to build out meander belt complexes (e.g. Carey, 1969; Page & Nanson, 1982; Smith *et al.*, 2009; Durkin *et al.*, 2020). Various field-based case studies have established that these two zones have distinct sedimentological characteristics (e.g. Hickin, 1979, 1986; Woodyer *et al.*, 1979; Page & Nanson, 1982; Makaske & Weerts, 2005; Smith *et al.*, 2009, 2011; Durkin *et al.*, 2020). Next to planform-based architectural identification of major elements of meander belts, vertical succession oriented facies models are deployed to identify and further fine-scale architectural variability within the point bar complex and abandoned channel fill (e.g. Allen, 1963; Miall, 1985). The point bar complex then is typically subdivided into lower and upper bar deposits, fining-upward into an overbank depositional unit, with abandonment-stage channel fills being an inset separate unit. (e.g. Allen, 1970; Bridge *et al.*, 1995; Sridhar & Patidar, 2005; Labrecque *et al.*, 2011; Durkin *et al.*, 2017). Architectural variability of abandoned channel fills is controlled by both hydrodynamic (for example, distal versus proximal facies) and sedimentological (for example, channel entrance angle and effectivity of plugging and shallowing and flooding regime) factors (e.g. Allen, 1965; Lewis & Lewin, 1983; Middelkoop & Asselman, 1998; Macklin & Lewin, 2003; Werritty *et al.*, 2006; Toonen *et al.*, 2012).

The fact that meandering rivers function in a variety of environments and geological settings (e.g. Saucier, 1994; Stouthamer & Berendsen, 2000; Morozova & Smith, 2000; Gibling, 2006; Durkin, 2017; Payenberg *et al.*, 2019) potentially has a direct impact on the distribution and characteristics of architectural elements. Differences in valley gradient, net incising versus aggradational situations, avulsion history and substrate configuration lead to a distinction between meander belt settings in fluvio-deltaic plains and in valleys (e.g. Nanson & Croke, 1992; Payenberg *et al.*, 2003; Stouthamer *et al.*, 2011; Fryirs *et al.*, 2016). In valleys,

meander activity and valley floor width are often constrained by terraced rims, colluvial bluffs and bedrock walls. That setting promotes the establishment of long-lived meander belts, the sedimentology of which is characterized by constant self-reworking (e.g. Słowik, 2016). This is in marked contrast with the laterally-unconstrained setting of the aggradational delta plains and lower megafans, in which individual meander belts tend to be created regularly by avulsions to function for a limited period of time until subsequent avulsions cause them to abandon before self-reworking would occur (Jones *et al.*, 1999, Stouthamer *et al.*, 2011, Kleinmans *et al.*, 2013, Latrubesse, 2015). Periodic repositioning of active channels, especially in combination with relative base level rise, promotes the development and preservation of isolated meander belt sands encased in floodbasin sequences (e.g. Weerts, 1996; Payenberg *et al.*, 2003; Fontana *et al.*, 2014). Moreover, substantial amounts of deposits recording gradual abandonment (syn-avulsion) and residual channel filling (post-avulsion) are created over a larger spatial extent (full reach lengths), than equivalent units such as plug bars and residual oxbow channel fills occupy in meander belts of alluvial valleys (Toonen *et al.*, 2012). This is not just because channel-belt deposits in avulsive deltaic settings preserve more easily, but also because their shorter lifespan increases the proportion of abandonment stage deposits relative to mature stage point bar deposits within these deltaic meander belts. The further downstream in an avulsive delta plain with multiple bifurcations, the shorter lived the meander belts will tend to be. In turn, this suggests that the sedimentary architecture of such meander belts is particularly suitable to study the products of steady meander translation, extension and rotation (Ielpi & Ghinassi, 2014), because between initiation and abandonment of fluvial activity the time available to complicate sedimentary architecture is limited.

The main research question addressed here is whether different stages of development during the lifespan of short-lived deltaic channel belts result in distinguishable sedimentary characteristics. To test this, the classic case of the Stuivenberg meander belt in the Rhine-Meuse delta was revisited (Berendsen, 1982; Stouthamer & Berendsen, 2001). This is an isolated channel belt of which the lifetime and general setting have been well-documented, and which forms an ideal case to develop planform architectural

division concepts, and allowed for the investigation of the causal relations between grain-size characteristics, meandering history and eventual preservation of abandonment as avulsion aftermath. In the present study the ‘architectural’ entities thus refer to parts of a deltaic channel belt resulting from subsequent stages of development of the channel belt over its lifespan, of which the scale corresponds with fifth-order surface bound architectural elements *cf.* Miall (1985, fig. 2).

Specific aims of this study were to: (i) identify specific grain-size characteristics for different parts of the meander belt across subsequent life-cycle stages; and (ii) determine to what extent observed architectural and lithological differences can be attributed to substrate composition, meander chronology and regional floodplain configuration. This allows us to explain differences in sedimentary characteristics within a meander belt preserved from subsequent stages of activity.

## STUDY AREA GEOLOGICAL SETTING

### Holocene Rhine-Meuse delta

The Holocene Rhine-Meuse delta (Fig. 1) is part of the Dutch coastal plain. It developed over the last 8500 years, when post-glacial sea-level rise reached full inundation of the North Sea (Berendsen & Stouthamer, 2000; Hijma & Cohen, 2011, 2019). The Holocene Rhine-Meuse delta has inherited its position due to glaciation events 150 000 years ago and peri-glacial river rerouting in the last glacial (Cohen *et al.*, 2002; Busschers *et al.*, 2007; Peeters *et al.*, 2016).

In the centre of the Rhine-Meuse delta, where the Stuivenberg channel belt is located, the Holocene deltaic wedge is several metres thick (e.g. Törnqvist, 1994; Gouw & Erkens, 2007) and buries a seaward dipping substrate of Late Pleistocene valley and valley-rim deposits. That substrate is mainly composed of gravelly sands left by laterally shifting braided rivers that existed during the Last Glacial Maximum (25 to 20 ka) (Busschers *et al.*, 2007). Increased aeolian activity in combination with sparse glacial vegetation during final Late Pleistocene stages resulted in deposition of aeolian cover sands in the terraced marginal areas of the Rhine-Meuse palaeovalley (Busschers *et al.*, 2005; Winkels *et al.*, 2021).

The development history of the Rhine-Meuse delta in relation to relative sea-level rise (i.e.

base-level rise) in essence comprised a *ca* 3000 year transgressive stage followed by *ca* 6000 years of highstand stage that is often split into a semi-natural and an anthropogenic overprinted first and second half (Berendsen & Stouthamer, 2000; Gouw & Erkens, 2007; Hijma & Cohen, 2011; Stouthamer *et al.*, 2011; De Haas *et al.*, 2018). From 8500 to 5500 years ago, relative sea-level rise at the river mouth dropped from 10 to 1 m kyr<sup>-1</sup> (Van de Plassche, 1982; Hijma & Cohen, 2010, 2019) and a barrier island coastline was establishing in a position that would become the Holland coast line (Beets & Van der Spek, 2000; De Haas *et al.*, 2018). The drowned palaeovalley initially accommodated a large tidal estuary that received the Rhine and Meuse rivers, which gradually filled with muds and peat (Hijma & Cohen, 2011; De Haas *et al.*, 2018). This transgressive system transformed into a highstand back-barrier delta. As rates of relative sea-level rise dropped further to background values <<1 m kyr<sup>-1</sup> and the Holland barrier system evolved on the seaward side, Rhine and Meuse deltaic deposition proceeded on the inland side. Central parts of that back-barrier area silted and freshened up, allowing for extensive peat formation. Extensive occurrence of ‘Holland Peat’ in the back-barrier area marks the arrival of this highstand stage of delta development, in which fluvial deltaic deposition and avulsion activity was relatively restricted to the Utrecht sector of the delta plain (Fig. 1; Berendsen, 1982). In that area, there are multiple generations of new avulsed river channels dissected and reworked transgressive-stage floodbasin sequences as well as pre-deltaic cover-sands and braided river deposits at shallow depths, and preserved as channel belt sand bodies (e.g. Stouthamer & Berendsen, 2001; Gouw & Berendsen, 2007).

A long tradition of mapping and dating campaigns of the channel-belt network (see also: Pierik & Cohen, 2020) has revealed its planform and avulsion history (e.g. Berendsen, 1982; Törnqvist, 1993; Berendsen & Stouthamer, 2000; Stouthamer & Berendsen, 2000; Gouw & Erkens, 2007; Stouthamer *et al.*, 2011; Pierik *et al.*, 2017). Delta-scale channel-style and architectural studies have classified the majority of the highstand channel belts as ‘confined meandering’, if not ‘straight’ (Makaske, 2001), meaning that widening of the channel belts during their periods of activity was hindered by the cohesive nature of the auto-compacting surrounding floodbasin substrate (e.g. Berendsen &

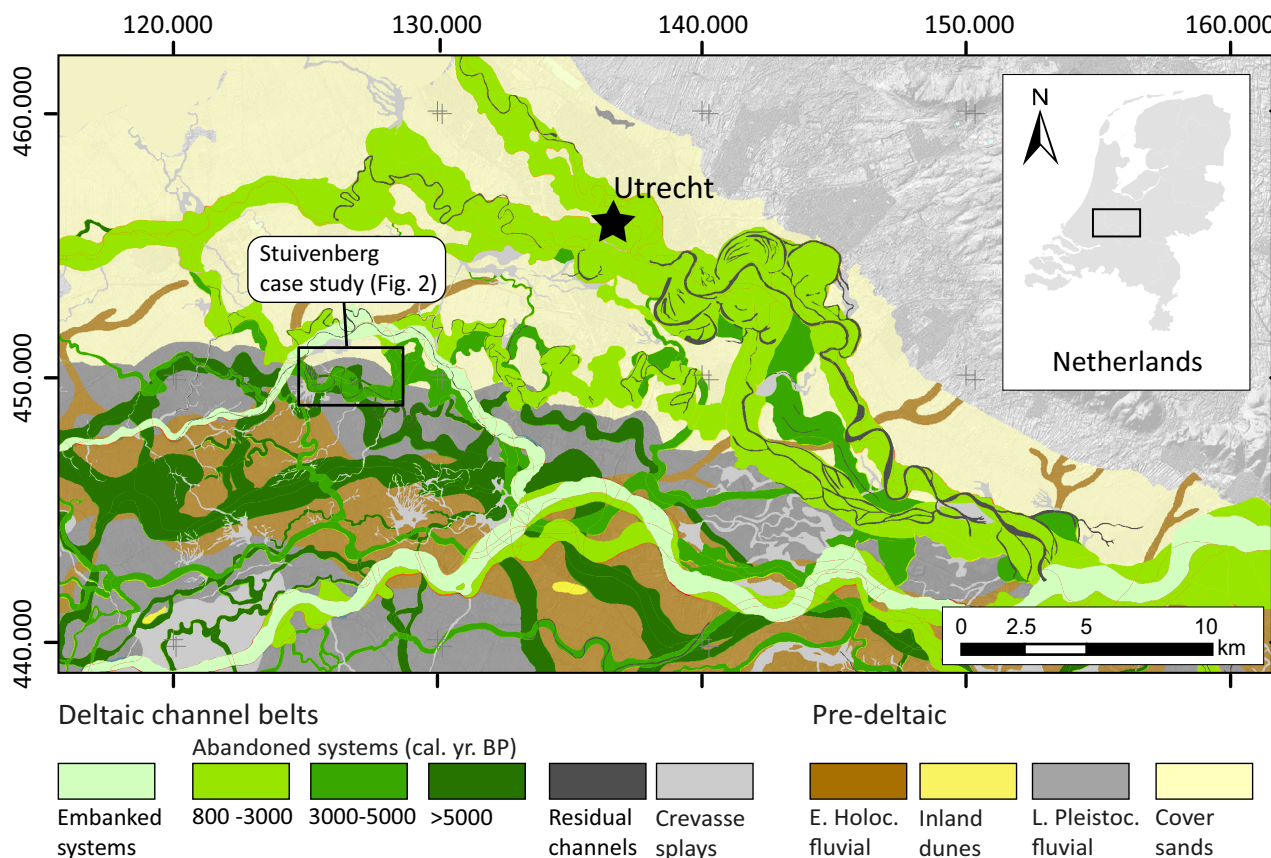


**Fig. 1.** Utrecht sector of the Rhine-Meuse delta, The Netherlands, showing various generations of meander-belt deposits (Cohen *et al.*, 2012; Winkels *et al.*, 2021), residual channel deposits (Berendsen, 1982; Pierik *et al.*, 2017) and location of the Stuivenberg channel belt (StvCB) case study area. Coordinates are according to the Dutch national RD-grid (EPSG:28992).

Stouthamer, 2000, 2001; Van Asselen, 2011). Dating control usually relied on a combination of sampling for absolute dating methods (mainly radiocarbon) at specific contacts of channel-belt architectural elements (for example, organics from base or residual channel) and dates obtained at archaeological investigations, corroboration with spatially continuous relative dating methods such as planform and vertical architectural-element cross-cutting relationships (Berendsen, 1982 – updated Törnqvist, 1993; Berendsen & Stouthamer, 2001; Gouw & Erkens, 2007; Cohen *et al.*, 2012).

### Stuivenberg channel belt

The Stuivenberg channel belt (StvCB) is a classic geological–geomorphological study site in the Utrecht sector of the Rhine-Meuse delta (Fig. 1). The StvCB is one of several active channel belts

that functioned in this area around 4000 years ago. The channel belts in the Utrecht sector are subdivided into the Utrecht and Linschoten river systems (*cf.* Berendsen, 1982), with the Utrecht river system having larger channel belts that carried the majority of the Rhine discharge, and the Linschoten river system made up by smaller channel belts with shorter-lived secondary branches. The alluvial ridge of the StvCB and its scroll bar and residual channel morphology are well-recognizable by the micro-topography and land use of the present polder landscape (Fig. 2A and B). The current collective dating evidence (Cohen *et al.*, 2012) puts the onset of StvCB fluvial activity shortly after  $3950 \pm 60$   $^{14}\text{C}$  BP (radiocarbon dates GrN-08704/UtC-01893), and well before  $3660 \pm 30$   $^{14}\text{C}$  BP (GrN-07967). Dates from the base of the residual channel fill, post-dating the channel abandonment, are  $3180 \pm 55$  (GrN-07576),  $3135 \pm 55$  (GrN-07581) and  $3195 \pm 55$

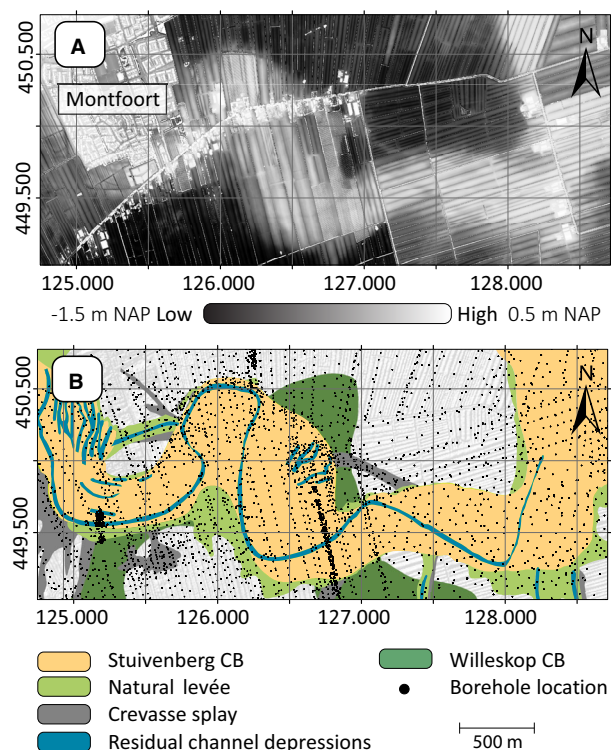


**Fig. 2.** (A) Topographic map (LiDAR: AHN3) of the Stuivenberg channel belt (StvCB) study area and (B) prior available data density (UU-LLG database) and planform reconstructions for: (i) the StvCB (Cohen *et al.*, 2012) and associated natural levée, crevasse splay (Pierik *et al.*, 2017) and residual channel elements (Berendsen, 1982); and (ii) the Willeskop channel belt (Cohen *et al.*, 2012).

$^{14}\text{C}$  BP (GrN-09263). Calibrated, the period of activity of the StvCB spans  $4.3 \pm 0.1$  to  $3.5 \pm 0.1$  ka cal BP, which is  $800 \pm 150$  years ( $1\sigma$ ).

The dense and rich digital archive of borehole descriptions and data archive UU-LLG (Berendsen, 1982; Berendsen & Stouthamer, 2001; Cohen *et al.*, 2017) formed the base of the Stuivenberg channel-belt mapping and age control of meander development in this study. Site accessibility and prior knowledge of floodplain-substrate configuration make the StvCB an ideal location for investigating the internal structure of channel-belt deposits and establishing the relationship of that with evolving boundary conditions. Through complementing the database with newly collected data on lithological composition, a detailed reconstruction was made of meander evolution during the period of activity of the StvCB for a 5 km stretch of which the morphology has been well-preserved (Figs 1 and 2).

## MATERIALS AND METHODS

### Subsurface datasets

Borehole description data, collected over several decades, was extracted from the UU-LLG database (Berendsen & Stouthamer, 2001; Berendsen *et al.*, 2007; Cohen *et al.*, 2017). In the study area (12 km<sup>2</sup>) this database contains *ca* 4000 digitized archived borehole descriptions (*ca* 330 per km<sup>2</sup>) that reach down to 10 m below the surface (<2 m = 80%, 2 to 5 m = 15%, >5 m = 5%). Borehole logs contain detailed descriptions of subsurface characteristics, routinely logged for 10 cm intervals for properties such as lithology (soil texture, De Bakker & Schelling, 1966), field-tested CaCO<sub>3</sub> content (decalcification depth; Berendsen, 1982) and, for sandy deposits, median grain-size classes ( $D_{50}$ ; determined against a field-reference; standard sieving classes, Berendsen & Stouthamer, 2001). The depth axis datum is NAP, the ordnance datum in The Netherlands, which is about equal to 20th century mean sea-level.

As a means of validating borehole data from the LLG archive, and to collect samples for grain-size measurements (*Grain-size analysis* section), 16 additional boreholes were cored and sampled during a field campaign in the summer of 2017 (average depth: 8 m), described with the same logging methods, and added to the UU-LLG database. These new boreholes were strategically positioned at 50 m spacing along two cross-sections perpendicular to the earlier mapped residual channel and channel-belt outlines, and about one full meander length apart (Fig. 2). Different hand coring methods were used to retrieve and sample sediments, depending on lithology and depth of the groundwater table. In the top soil, an Edelman soil auger was used. Below the groundwater table, for fine-clastic and organic deposits a gouge auger was used, while in water-logged sandy deposits the Van der Staay suction corer was deployed (Oele *et al.*, 1983). In new core descriptions and a subset of corings from the UU-LLG database, attention was paid to the potential presence and traceability of inclined heterolithic stratification (IHS; lateral accretion, epsilon cross-bedding) or other sedimentary features. Within well-described individual cores, and positional context of the cores within channel-belt sands, likely IHS-sets are indeed spotted in the upper half of the sand body. However, the coring spacing and descriptions in the UU-LLG database

proved to be insufficient for fully identifying and tracing IHS set-structures laterally, or to determine transverse bed slope angles. In addition, the quality of available cores did not allow for identification of other sedimentary features. Therefore, this aspect was not investigated in any further detail.

## Mapping architectural elements

### *Planform extent and internal division*

Existing profile type criteria were used to classify boreholes and to map the boundary between the StvCB channel belt and its levée wings from the floodbasin. These criteria consider the upper 2 m of the borehole descriptions, and include rules on soil textural composition and CaCO<sub>3</sub> content, in combination with hydromorphic features (following Berendsen, 1982; Pierik *et al.*, 2017).

Within the StvCB, the residual-channel fill deposits sharply contrast the surrounding channel-belt sands. Hence, boreholes showing sandy lithologies ('point bar complex', e.g. Hesselink *et al.*, 2003; Gouw & Berendsen, 2007) are grouped into different profile types than those with fine-grained, irregularly laminated sediments ('residual channel fill', e.g. Toonen *et al.*, 2012) at shallow depths (1 to 4 m; for example, Fig. 2B). Importantly, the morphologically and lithologically traceable residual channel, is a narrow feature that matches only part of the original palaeochannel width (Berendsen, 1982; Hesselink *et al.*, 2003; Gouw & Berendsen, 2007). Where the StvCB dissected older generations of channel belts, additional criteria came into play such as comparison of elevation of the top of sand and preserved surface morphology (e.g. Berendsen & Stouthamer, 2001).

Increased borehole density and upgraded LiDAR data (Actueel Hoogtebestand Nederland 2, 2010; Actueel Hoogtebestand Nederland 3, 2017) allowed to locally revise the exact positioning of the natural levée/floodbasin and channel-belt compared to earlier iterations of mapping (studies cited above). Also, a further distinction was made in the sand body mapping to distinguish channel sands of actively shifting meanders (mature stage) from sandy and non-sandy deposits in final stages of river functioning (abandonment stage). Where previous studies mapped the total sand body width, our map legend separately indicates: (i) cross-stratified, IHS-bearing sandy channel-belt deposits associated with channel shifting; (ii) cross-stratified

sandy deposits associated with channel infilling (adjacent to the narrow residual channel landform); (iii) fine-clastic and organic deposits associated residual channel filling; and (iv) proximal overbank deposits directly overlying channel sands, associated with crevassing and natural levée formation at bank-full exceeding stages.

The cross-sections also depict the deposits encasing the StvCB, grouped under 'post-StvCB floodbasin deposits' (distal overbank clays mainly), 'Pre-StvCB floodbasin deposits' (organic-clastic sequences, alternating proximal and distal overbank deposits), 'Older deltaic channel belts' (sandy within-channel deposits with some overbank topping) and 'Pre-deltaic substrate' (palaeovalley channel deposits in the south, cover-sand blanket over older fluvial terrace sands in the north; *Study area geological setting* section). Vertical separation of StvCB sands from substrate sands is based on Van der Staay borehole observations on lithology. These include overall contrasts between StvCB and substrate sands such as on colour, CaCO<sub>3</sub> content, grain-size and sorting variations over 1 to 2 m above and below the contact, as well as on thalweg (channel lag) indicators such as markedly increased admixture of gravel and concentrations of rolled clay, peat and wood clasts. Such substitutes for recognition and tracing of the actual erosional surface (which borehole logging quality and spacing do not allow for) is regarded accurate to  $\pm 0.3$  m.

### *Residual channel mapping and ridge–swale reconstructions*

Verifiable in borehole profiles, LiDAR imagery allows to trace large fragments of the residual channel as an elongated (semi-)continuous sinusoidal depression (Berendsen & Volleberg, 2007). Where agricultural fields have been levelled and borehole data density is low, the position of the residual channel was hard to determine. In such locations the residual position was reconstructed as a continuous line connecting the known channel positions at either side.

Ridge–swale scroll morphology further served as indicative record for past meander migration, allowing to divide the point bar complex spatially in concave and convex accretion zones. Because the StvCB is *ca* 3500 years abandoned and buried by younger delta plain deposits, the ridge–swale morphology as seen at the surface today is strongly subdued. Nevertheless, arcuate swale depressions can still be identified within

the LiDAR imagery, paralleling the more continuous depression of the residual channel (Fig. 2A). Furthermore, for the most densely borehole data covered parts of the channel-belt, subsurface ridge–swale topography is identifiable in cross-section plots (Supinfo S1).

#### Abandonment stage architecture concept

In this study the ‘active stage’ comprises avulsive initiation and maturation of the meander belt, up to and including the time that it carried its maximum discharge. What is labelled ‘the abandonment stage’ comprises near-final last episodes of river activity, from the moment it starts losing discharge triggered by a new upstream avulsion, but still continues to carry significant flow (Stouthamer *et al.*, 2011; Kleinhans *et al.*, 2011; Toonen *et al.*, 2012). Abandonment stage deposition is followed by a ‘post-abandonment stage’ (formation of the residual channel element discussed above). The width and position occupied by abandonment-stage sand and the residual channel element of a channel belt together (‘abandoned channel zone’) represent the width of the original mature stage channel at the moment that an upstream avulsion process began. Because in this study the goal is to confront planform and cross-sectional architectural division with independent grain-size data, a protocolized method was developed to deploy the abandonment staging insights into channel-belt mapping (next sections).

#### Abandonment stage width approximation

Because the abandoned channel zone width is wider than just that of the final residual channel, it could not be measured from the LiDAR imagery depression directly. Hence, an explorative approach was used to establish an approximated width of the abandoned channel zone ( $W_{AbCh}$ ) using an empirical relation (Eq. 1; adopted from Hobo, 2015; Candel *et al.*, 2018). It relates active width to a channel depth, derived from borehole transects, and transverse bed slope angle (Fig. 3).

$$W_{AbCh} = 1.5 \frac{\text{Channel depth}}{\tan(\text{transverse\_bed\_slope})} \quad (1)$$

Thalweg channel depth during bank-full conditions was determined from the thickness of the channel belt (channel base contact to top levée deposits, Figs 6 to 9). Across the width of the channel belt it was at least 7 m, and locally

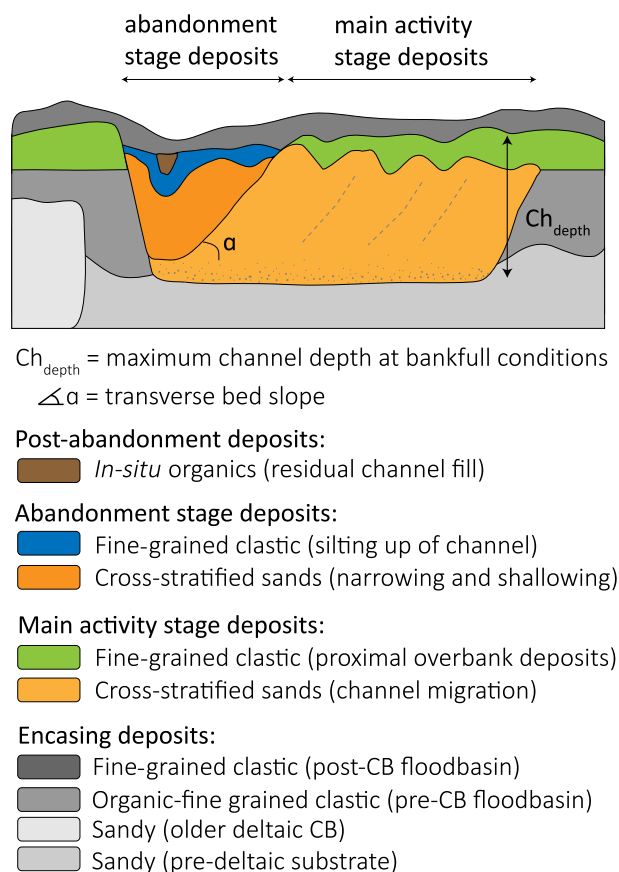


**Fig. 3.** Conceptual cross-section of abandoned deltaic channel belt architectural elements and encasing floodplain-substrate deposits. Input variables for Eq. 1 (transverse bed slope and channel depth) indicated.

scoured to 9 m. Note that channel depth as an input for Eq. 1 has a bankfull stage connotation in original applications, i.e. an inundation level reached and exceeded a few weeks per year. The channel width that is sought in our mapping (planform division of the upper point bar) is an approximate width at mean-annual discharge (i.e. year-round wetted area), when the sandy river bed and its accompanying youngest swales were inundated but higher elevated parts of the levées (non-sandy facies) were not.

The transverse bed slope could not be determined from augered cross-sections directly. Hobo (2015) determined a local transverse bed slope for a single cross-section of the Hennisdijk channel belt (8.3°) that is of similar age, size and setting, located some 20 km to the south-east. The transverse bed slope is expected to vary along the course of a meandering channel

**Table 1.** Parameter space exploration for Eq. 1.

Transverse bed slope (°)	Channel depth (m)	Channel width (m)
6	7	99.9
6	9	128.4
10	7	59.6
10	9	76.5

with bending and straight thalweg sections (e.g. Julien & Wargadalam, 1995). In order to take into account potential natural variability, a range of 6° to 10° was used in range-finder calculations when determining the potential width of the abandoned channel (Table 1). From that exercise a rounded middle-ground value of 100 m was deemed representative for the StvCB abandoned channel width. The authors then operationalized this value by plotting an abandoned channel zone of that width around the LiDAR-supported residual channel position and confronting it with lithological data in our main cross-sections (*Channel-belt structure* section).

#### Backtracking channel centre-lines

In order to study meander migration during the active stage of the StvCB, a comparable point on each individual meander needs to be identified (Fig. 4 – cf. Russell, 2017). The LiDAR-based, borehole-data aided mapping of ridge–swale morphology (*Residual channel mapping and ridge–swale reconstructions* section) provides the input to reconstruct estimated centre-line positions representing former trajectories of the palaeochannel in the middle and early activity phases of the StvCB, besides that of the final stage represented by the centre-line of the abandoned channel zone. Tangent lines ( $M_{\text{tangent}}$ ) drawn from the channel position lines connect two points on the immediately upstream and downstream meanders that mark the upstream and downstream break of each individual meander ( $M_{\text{break}}$ ). The meander bend apex ( $M_{\text{apex}}$ ) is defined as the point along the channel position line that is furthest from  $M_{\text{tangent}}$  (Fig. 4). Tracing corresponding meander apexes along the different activity phases is a way of (back)tracking meander evolution and channel-belt formation, and allows for characterization of meander bend migration in terms of translation, rotation and expansion (e.g. Ielpi & Ghinassi, 2014). For the most upstream and downstream meanders of the studied reach, tangent lines and  $M_{\text{apex}}$  are more

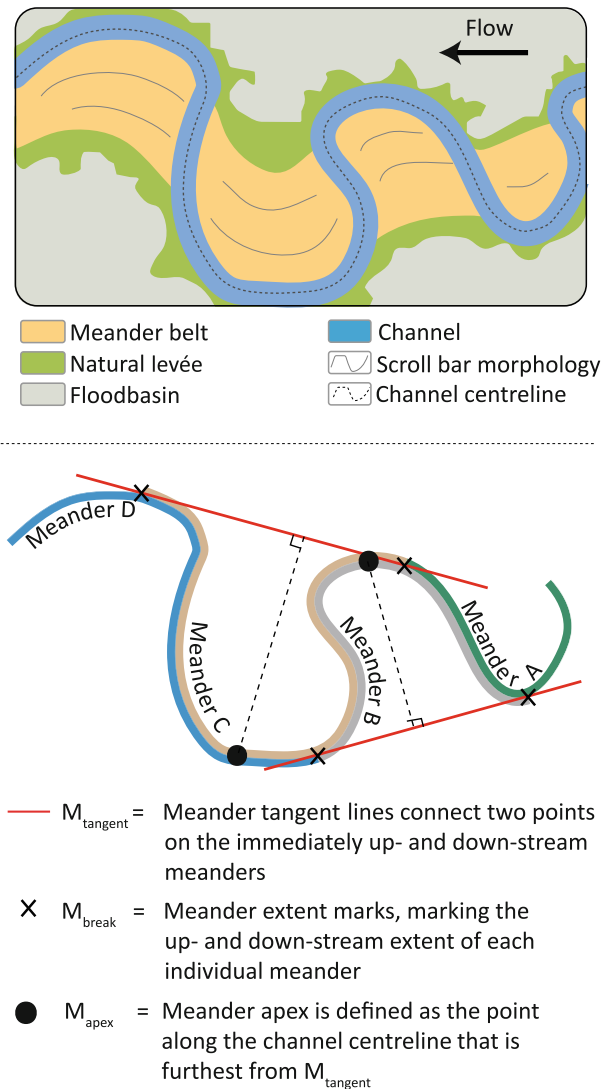


**Fig. 4.** Conceptual meander planform reconstruction and identification of overlapping meanders and corresponding meander apex through the use of meander tangent lines after Russell (2017).

tentatively drawn, as the method has to extrapolate beyond the study area edges.

#### Grain-size analysis

##### Laboratory analysis new samples

From six recent boreholes in cross-section B, 386 samples were analysed for grain-size distributions. The analysis was performed using a HELOS Laser Particle Sizer (Sympatec GmbH, Clausthal-Zellerfeld, Germany), which has a measuring range which lies between 0.15  $\mu\text{m}$  and 2000  $\mu\text{m}$  transformed into 56 grain-size



classes. In order to prevent clogging, all samples were pre-sieved over a 1400  $\mu\text{m}$  sieve. Residual material was pre-treated to remove organic matter and carbonates which could potentially impact the grain-size analysis. All samples were boiled in a 20%  $\text{H}_2\text{O}_2$  solution which dissolved all of the organic matter and further treatment with 10% HCL dissolved all carbonates. Finally, *ca* 300 mg of  $\text{Na}_4\text{P}_2\text{O}_7 \cdot 10\text{H}_2\text{O}$  was added to further disperse grains (Konert & Vandenberghe, 1997). Calculation of various grain-size, scale and shape statistics ( $D_{50}$ , sorting, skewness and kurtosis) gave a broader insight into the entire grain-size distributions and were done using the Analysize algorithm (Paterson & Heslop, 2015). A supplementary data file stores the measurement results (Supinfo S2).

### Grain-size mapping

The ample number of shallow boreholes hitting the top of the sand within the study area allows for the spatial investigation of median grain-sizes within the various architectural elements. To balance the spatial coverage of boreholes, the average compositions of the upper half metre of sandy substrate were investigated. Multiple preparatory actions were performed on the UULLG database records (Winkels *et al.*, 2021: their appendix C) to extract representative central  $D_{50}$  values based on the geometric mean of the class boundary values (e.g. Krumbein, 1934; Blott & Pye, 2001). Interpolation of the  $D_{50}$  values was done by quadratic inverse distance weighting using a maximum of the five nearest points. Grain size in the abandoned channel zone was interpolated separately from the rest of the StvCB point bar complex.

## RESULTS

### Planform architecture

The mapping of the StvCB active stage and abandonment stage elements covers 2.5 meander wavelengths, allowing to study three subsequent alternate meanders in full (Meanders 2, 3 and 4), and two more as upstream and downstream bounds (Meanders 1 and 5). The sinuosity of the studied meanders seen in the abandoned channel outline varies strongly, whereas the majority of the StvCB is about 300 m wide over most of its length within the studied area. The exception is the central part of the study area where the

channel belt widens to 700 m (Meander 3 – Fig. 5).

The abandoned channel zone is mapped as 100 m wide (*Abandonment stage width approximation* section), which is one third to one fifth of the StvCB characteristic cross-sectional width. The residual channel has a width of *ca* 30 m, which is one third of the estimated channel width by the end of the active stage. Over most of its length the abandoned channel zone follows the edge of the channel belt, crossing over at four locations (Fig. 5).

Planform investigation of the overbank deposits (i.e. natural levée wings and crevasse splays) shows a clear asymmetry between the northern (*ca* 75 m wide levée wings) and southern (*ca* 150 m wide) flanks of the StvCB alluvial ridge. This is also seen in the size of crevasse splay features (Fig. 5). At the northern flank, the crevasse splays are markedly smaller (i.e. less developed) compared to those at the south (of which that leaving Meander 5 was the most mature; see Stouthamer, 2001). Apparently, the gradient advantage of flood water overtopping the levée and producing crevasse splays was smaller in a northward direction than towards the south.

### Channel-belt structure

A series of cross-sections (Figs 6 to 8) reveal the internal structure of segments of the StvCB (Fig. 6). At cross-section A through Meander 5, the StvCB is *ca* 300 m wide with the abandoned channel zone positioned along the southern channel-belt edge (Fig. 5). The base of the StvCB channel deposits, identified from channel lag facies (boreholes 201701.014–015–016) is 1 m deeper in the abandoned channel zone (base at –8.5 m NAP) than in the active zone (base at –7.5 m NAP).

Sandy deposits from the active stage of the StvCB show comparable sedimentary sequences along the entire cross-section. Lower bar deposits, ranging between three and five metres thick, are characterized by highly variable  $D_{50}$  values, fluctuating between 400  $\mu\text{m}$  and 800  $\mu\text{m}$ , without any clear vertical trend (Fig. 6). The upper bar deposits show less variation in  $D_{50}$  values and a clear fining-upward (FU) trend, continuing into the natural levée deposits (Fig. 6). The thickness of this FU sequence increases in a northward direction by *ca* 1 m. Cross-verification between planform reconstructions of the abandoned channel and lithological data

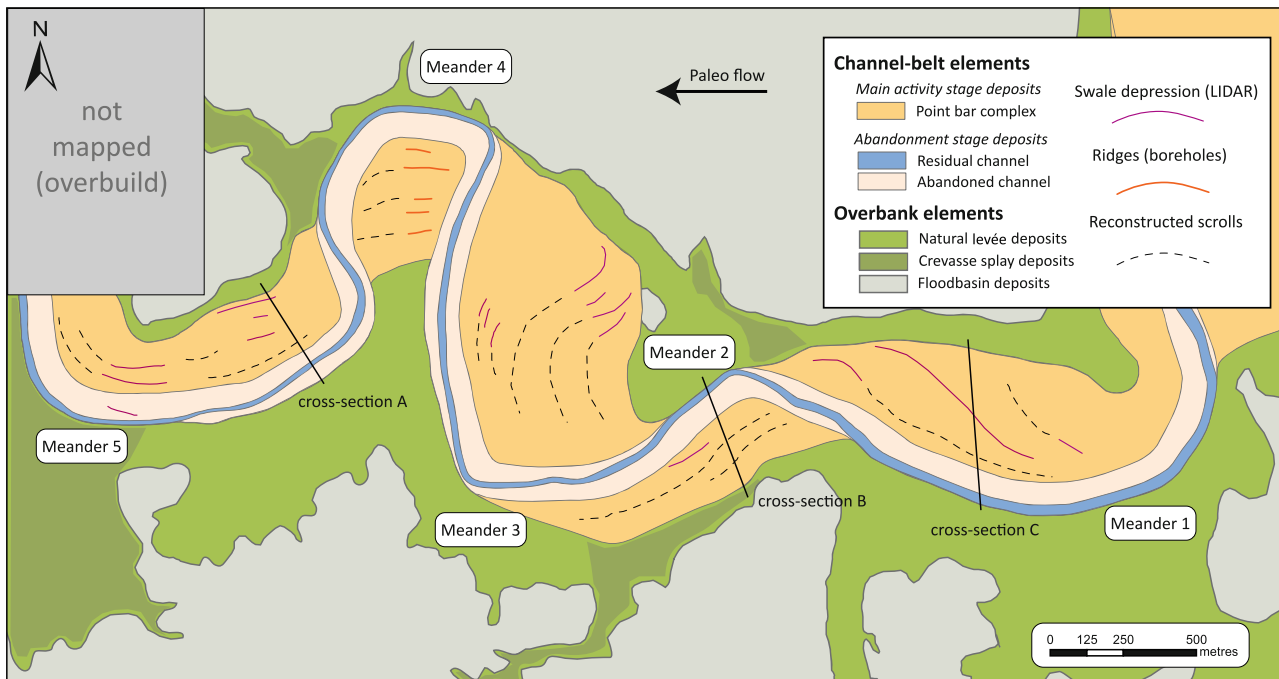


**Fig. 5.** Planform reconstructions of main activity and abandonment stages and reconstructed ridge swale morphology. Locations of individual cross-sections (Figs 6 to 8) and isolated boreholes (Fig. 11) are also depicted.

reveals that the characteristics of sandy deposits from the abandoned channel zone stand out as a clear dichotomy. At the base, they show highly variable  $D_{50}$  values, fluctuating between 300  $\mu\text{m}$  and 800  $\mu\text{m}$  and clear FU. Above  $-5$  m NAP, they show a more gradual fining-upward signal. Fine-clastic deposits then top the sandy channel infill, containing sandy loam intercalations and ample plant remains.

Also along cross-section B, which stretches Meander 2, the StvCB is *ca* 300 m wide. Here abandonment phase elements are situated along the northern edge. Beyond the southern edge, a crevasse splay system is present (Fig. 5). The thickness of channel-belt deposits varies strongly across the section, with thickest sequences found near the margins of the channel belt (Fig. 7). Here, borehole 201701.007 penetrated the entire channel belt, and identified channel lag deposits at  $-7.8$  to  $-8.6$  m. In the centre of the channel belt, borehole 201701.005 at  $-7.2$  m also bases the channel belt. Several subfacies are identified within the active zone sands (Fig. 7). Variability in  $D_{50}$  values allows to make a distinction between the southern and northern sections of the active stage sandy body. In boreholes 201701.005–006–007 (south), below  $-5$  m,  $D_{50}$  is fairly stable, varying between 300  $\mu\text{m}$  and

450  $\mu\text{m}$  only. In boreholes 201701.003–004 (north), variation in  $D_{50}$  values of sandy deposits below  $-5$  m is much greater: between 300  $\mu\text{m}$  and 800  $\mu\text{m}$ . Upper portions of the channel-belt sand (above  $-5$  m NAP) show clear vertical grain-size trends, but again a difference between the northern and southern sides exists. Boreholes 201701.005–006 show a coarsening-upward (CU) trend while boreholes 201701.003–004 show a FU trend.  $D_{50}$  variability in the majority of the boreholes (201701.002–003–004–005–006) is limited (varying between 400  $\mu\text{m}$  and 600  $\mu\text{m}$ ), only the southernmost borehole 201701.007 shows considerably more variability (varying between 300  $\mu\text{m}$  and 700  $\mu\text{m}$ ). In the central part of the section, the top 1 to 2 m of sandy deposits is markedly coarser ( $D_{50} > 800$   $\mu\text{m}$ ), more poorly sorted and characterized by a gradual FU trend. The lower bounding surface of these coarse deposits is characterized by a sharp transition indicative of its erosive nature. The upper bounding surface is characterized by a sharp transition to overlying levée deposits. In the abandoned channel zone, the upper part of the sedimentary sequences in cross-section B are similar to those in cross-section A. Borehole 201701.002 shows a sequence characterized by relatively stable  $D_{50}$  values but with a clear FU trend in the upper part

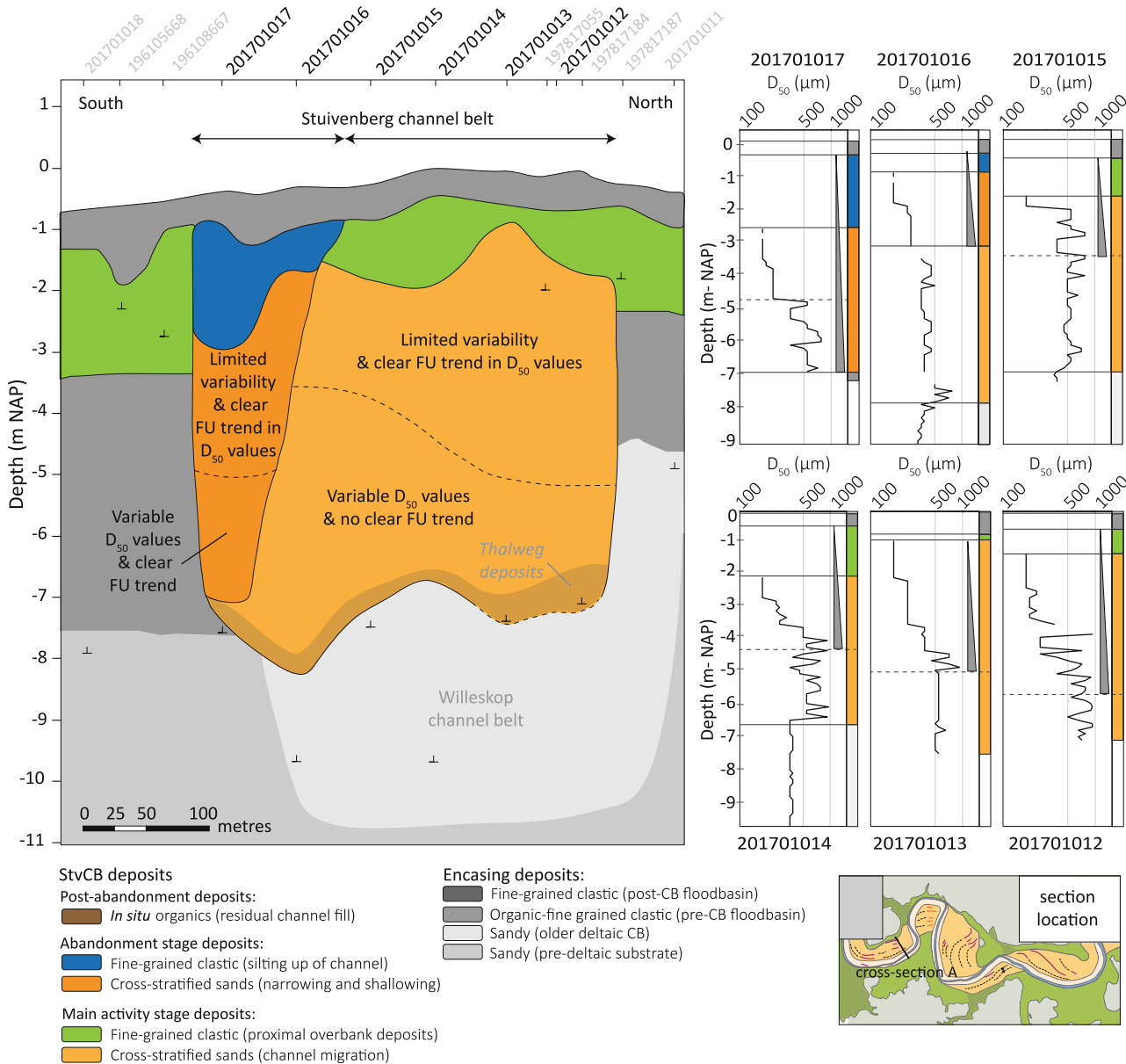


**Fig. 6.** Cross-section A: Lithological cross-section showing the Stuivenberg channel belt (StvCB) architectural build-up and corresponding sedimentary characteristics and trends as well as encasing sediments.

of the abandoned channel fill that is topped by fine-grained clastic deposits, locally grading into peaty beds (Fig. 7). In addition to having a smaller median grain size, abandonment stage sands contain more silt (*ca* 5%) than active stage sands (<1%), and for that reason also are less well-sorted (Supinfo S2). Below the abandonment stage sand at -4.3 m NAP, an organic interval is locally present, that terminated borehole 201701.002. Therefore, the exact depth, position and geometry of the channel could not be

established: the interface between the cut-bank wall and channel floor may be more irregular than drawn in Fig. 7.

Cross-section C, which was constructed using legacy borehole descriptions only, stretches *ca* 500 m over Meander 1, where the abandoned channel zone is situated along the southern edge of the channel belt (Fig. 5). Analysis of the sand characteristics is less detailed, but again the deeper part of the sand seems to lack vertical trends in median grain size, despite

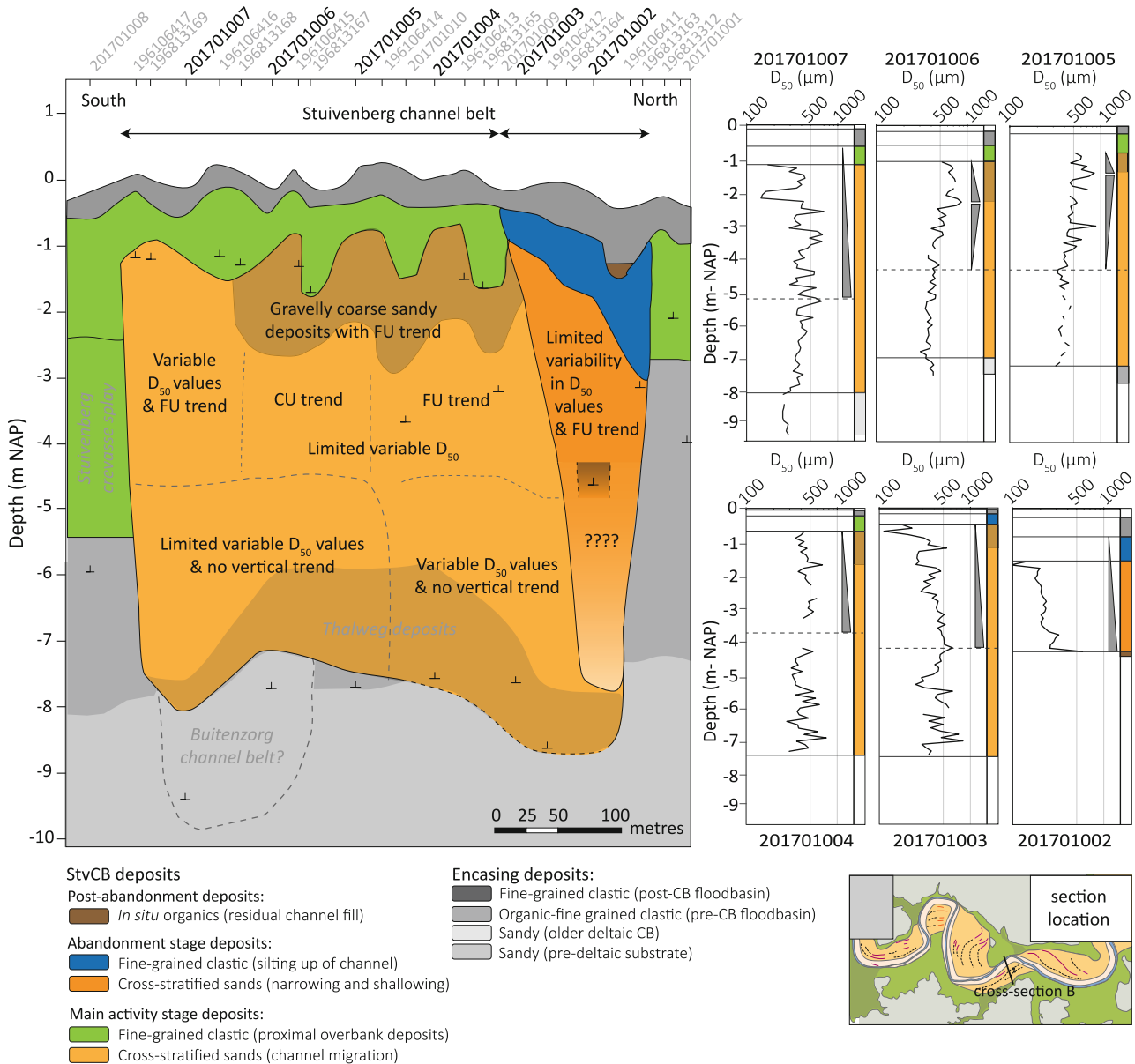


**Fig. 7.** Cross-section B: Lithological cross-section showing the Stuivenberg channel belt (StvCB) architectural build-up and corresponding sedimentary characteristics and trends as well as encasing sediments.

considerable  $D_{50}$  variability contrasts (compare boreholes 199002.122 and 199002.120). Variability in  $D_{50}$  drops at shallower levels but most boreholes do not show vertical trends in median grain size (Fig. 8). An enigma in this cross-section, is a thick sequence (nearly 9 m) of fine-grained clastic deposits found at the northern edge of the StvCB (borehole 199002.123). In the other cross-sections and the majority of the further mapped channel belt, sands mark the channel-belt edge opposite

the abandoned channel zone (Fig. 5). Investigation of floodplain deposits beyond the channel-belt edge does not reveal any crevasse splay systems active in this subreach. Hence, the fine-grained sequence is likely deposited during the active stage of the StvCB. This irregularly-laminated loamy facies appears to have accreted in the wake of the scrolls of Meander 1 (Fig. 5), a phenomenon also recognized locally in other similarly aged channel belts in the central Rhine-Meuse delta ('concave-bank

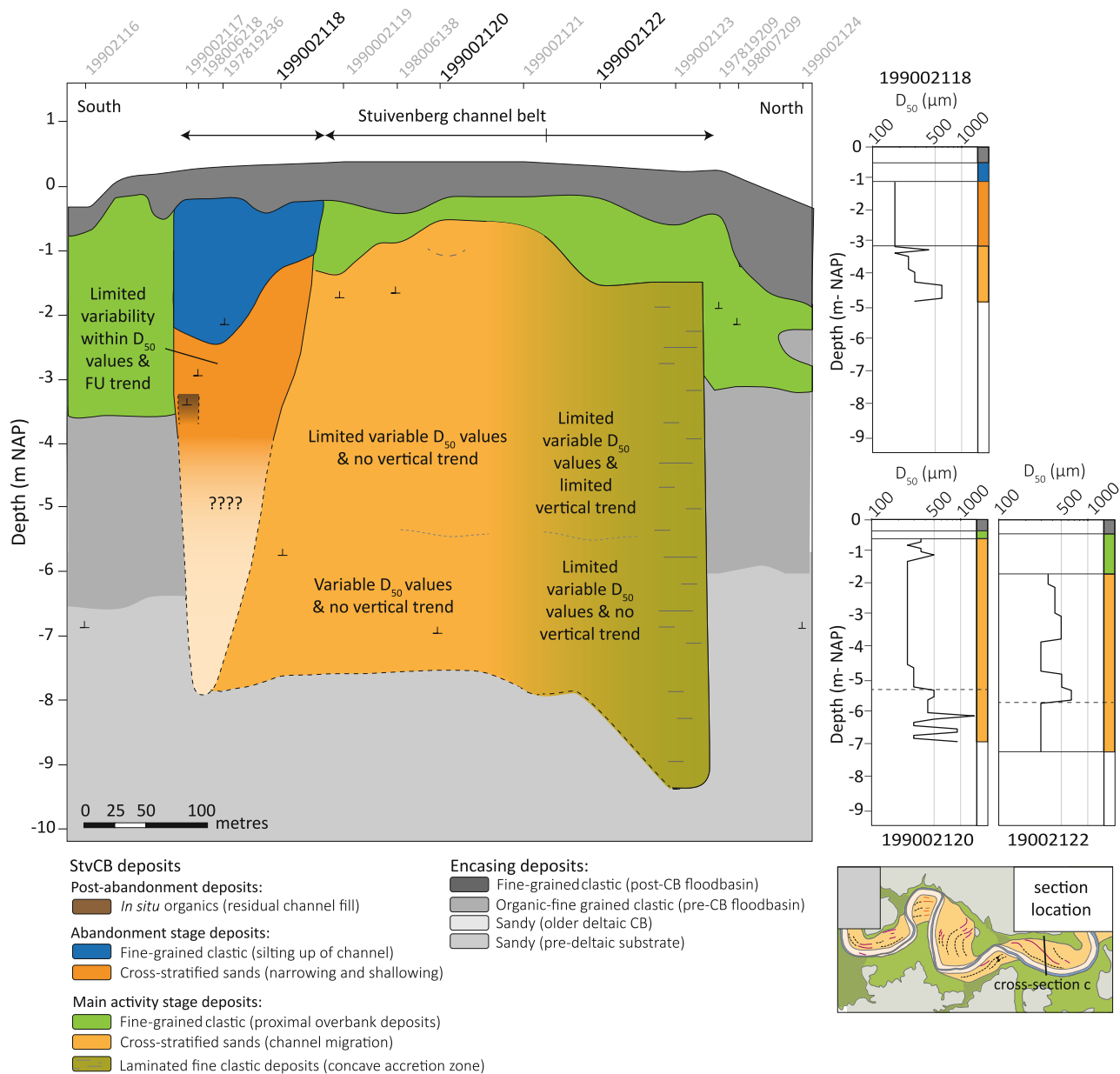


**Fig. 8.** Cross-section C: Lithological cross-section showing the Stuveberg channel belt (StvCB) architectural build-up and corresponding sedimentary characteristics and trends as well as encasing sediments.

bench accretion' *cf.* Makaske, 2001). In the abandonment stage zone, cross-section C shows a similar sequence as cross-sections A and B, with the abandonment stage sands showing steady FU for the upper part of the abandoned channel fill (Fig. 8). As in cross-section B, the exact outer positions and basal geometry of the sand body remain unestablished. Also here organic intervals have terminated some of the deeper reaching boreholes (for example, 199002.117 at  $-3.2$  m).

### Grain size of upper sandy deposits

Where cross-section B traverses Meander 2, a patch of very coarse sand ( $>850$   $\mu\text{m}$ ) is encountered at the top of the channel belt sand body (Fig. 7: between boreholes 2001701.002–006,  $-1.0$  to  $-2.5$  m depth). This coarse zone can be traced for some distance in planform in the vicinity of the section but varies strongly in thickness (1 to 3 m). Such patches of shallow coarse sand also show up

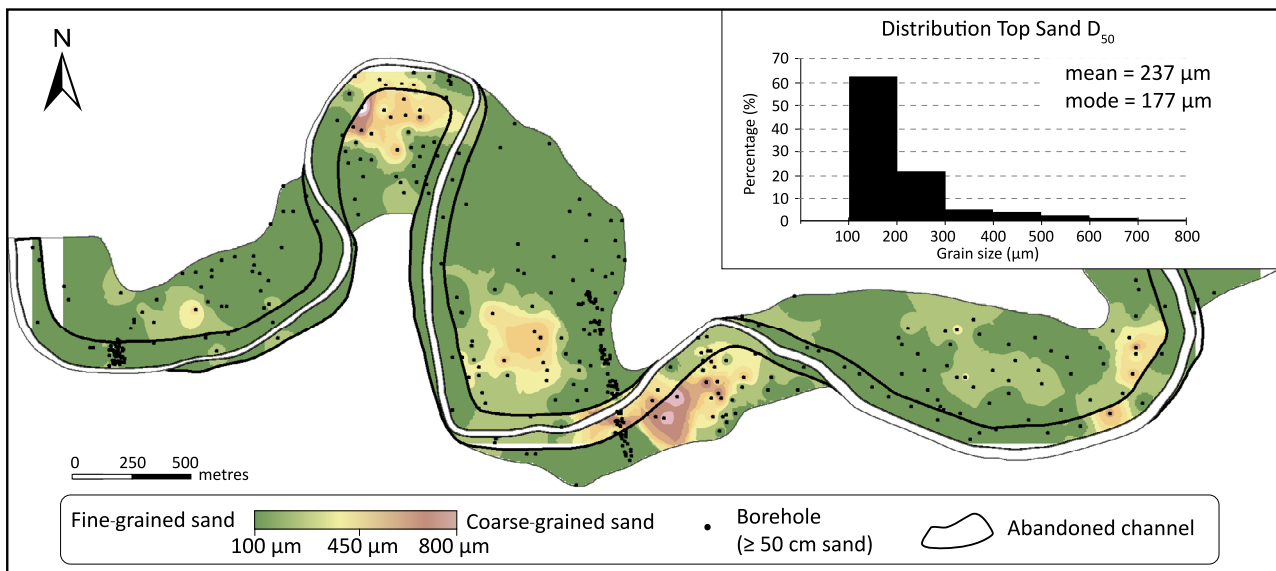


**Fig. 9.** Planform reconstruction of average  $D_{50}$  values for the upper (0.5 m) sandy deposits of the Stuivenberg channel belt (StvCB) main activity stage and abandoned stage and corresponding histogram showing the distribution of top sand averaged grain-size values.

in the other meanders (Fig. 9). Coarse-grained patches also occur within the abandoned channel zone, adjacent to and/or just downstream of the coarse-grained patches in the point-bar complex (Fig. 9).

For the lower point bar deposits, no 2D patterns of grain size could be determined, because only 5% of the borehole data reached deep enough to log them. Discussion of grain-size trends in lower and upper point bars therefore relies on the high-resolution sampled transects A and B (Figs 6 and 7).

### Meander evolution

Figure 10 shows estimated backtracked locations of the early (estimated 4.2 ka cal BP) and middle (*ca* 3.9 ka) lifecycle positions of the StvCB palaeochannel, allowing to interpret meander evolution and link this to the architectural structure and grain sizes of the channel belt.

Former  $M_{\text{apex}}$  positions suggest migration of Meanders 2 and 3 to have occurred in a downstream direction mainly, i.e. as translated meanders. This is the expected behaviour for deltaic channel belts such as the StvCB (*Holocene Rhine-Meuse delta* section), given that they establish their course in a 5 m thick body of cohesive floodbasin substrate (Figs 3 and 6 to 8). At the channel-belt boundaries the downstream

translation resulted in the formation of concave-bend accretion zones (Fig. 10).

Tracking of the  $M_{\text{apex}}$  positions of Meander 4 shows a more complex downstream migration pathway, indicating rotation besides translation. Interestingly, between Meanders 3 and 5, the path of the StvCB coincides largely with that of the older Willeskop channel belt (Figs 2 and 10). Here the channel initially encountered a relatively shallow sandy substrate, which was less cohesive than the upstream floodbasin material, which can explain the relative widening of this section of the channel belt and the relatively shift translation orientation of Meander 3. Also, the rotation shown by Meander 4 and the westward redirection towards Meander 5 developed owing to the less erodible substrate in the underlying bend of the Willeskop channel belt. The trajectories of  $M_{\text{apex}}$  of Meanders 1 and 5 suggest modest outward migration perpendicular to the channel-belt axis. These parts of the channel belt remained the narrowest, implying that these bends increased their curvature and sinuosity only slowly.

### Concave accretion zones

Figure 10 maps zones within the channel belt which, based on ridge–swale scroll evidence and meander evolution reconstructions, were

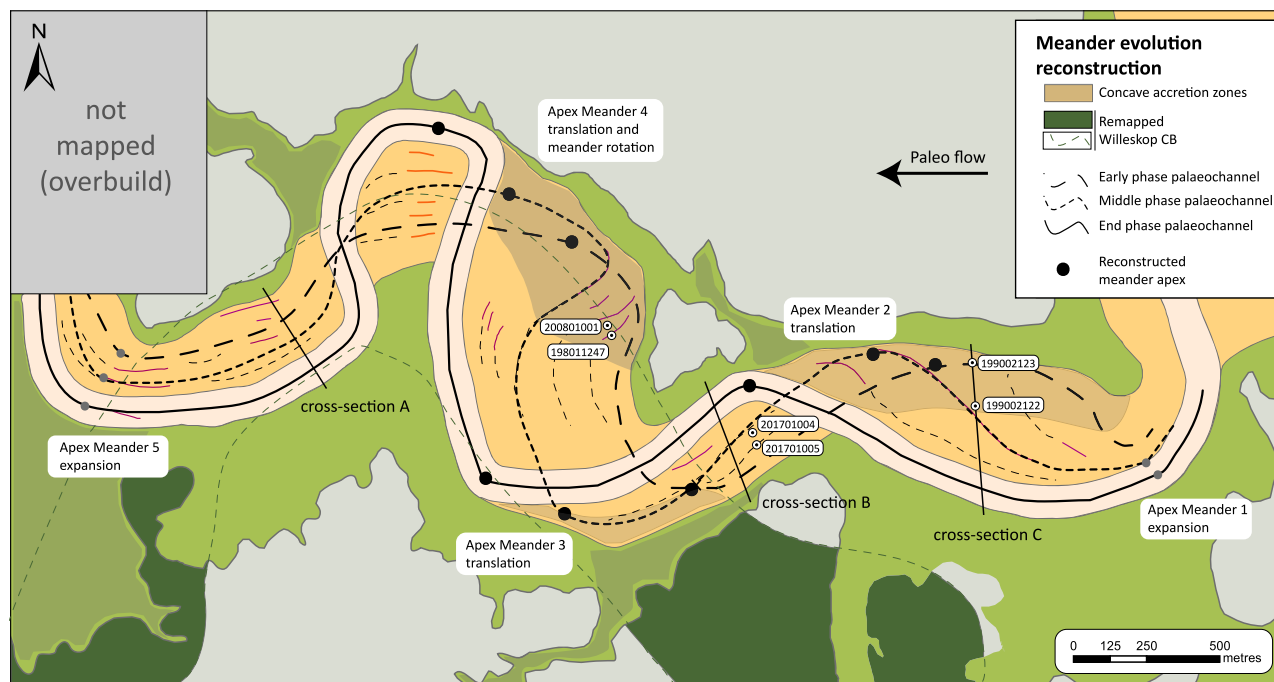


**Fig. 10.** Reconstruction of meander evolution of the Stuivenberg channel belt (StvCB). Dashed lines show the estimated location of the palaeochannel during the early, middle and final phase of the StvCB.

formed by concave bar or bench accretion. Investigation of deeper boreholes (>5 m) within the concave accretion zones of Meanders 3 and 1 reveals a remarkably variable composition including both sandy and non-sandy sequences (Fig. 11). This is well shown by borehole pair 198011.247 and 200801.001, located just 25 m apart in a densely cored area showing concave scrolling in LiDAR topography (Fig. 5) and formed by Meander 3 early in StvCB history (Fig. 10). The first borehole is dominated by fine-grained deposits, the second one by fine to medium-grained sand; this is notably finer than at typical convex-accretion locations (for example, boreholes 201701.004–005 from cross-section B in Fig. 11). From the concave accretion zone of early phases of Meander 1 traversed by cross-section C, exemplary fine-grained borehole 199002.123 is paired with sandy borehole 199002.122 from just 75 m downstream in the channel belt. The first has a very thick (>9 m) fine-grained clastic sedimentary sequence, reaching to below common channel-belt base suggesting a degree of local scouring which is consistent with established ideas on formation of eddy accretion zones (Smith *et al.*, 2011; Durkin *et al.*, 2020). The latter is dominated by dominantly sandy deposits (Fig. 11), finer

grained and less variable in  $D_{50}$  than the boreholes within the convex-accretion zone.

## DISCUSSION

### Grain-size variability in lower and upper point bar deposits

Along-transect grain-size variations observed in the Stuivenberg channel belt (StvCB) reflect: (i) differences in flow and sediment sorting within a river channel; and (ii) successive preservation of specific sections of the meander belt as the channel migrated. The absence of any vertical trends in median grain size within the lower parts of active-stage point bar complexes (Figs 6 to 8) indicates a fairly equal mobility of all encountered size fractions. In contrast, the upper parts of the point bar deposits typically show a FU trend in median grain sizes, explained as the outcome of more selective transport by the secondary flows that evacuate relatively finer sediments from the bed load carried in deeper parts of the channel and let this accrete at bar tops (Figs 6 to 8). Still, differences exist in the variability in median grain sizes within and between the three transects

(Figs 6 to 8). This variability is discussed here and related to: (i) overall progressive changes in incoming discharge and sediment over the lifecycle of the StvCB; and/or (ii) more-local morphodynamic feedback effects at the bar-complex scale, owing to shape shifting of the meandering channel course.

*Lower bar deposits* in cross-section B show a dichotomy between the younger northern ( $D_{50} \approx 600 \mu\text{m}$ , highly variable) and older southern ( $D_{50} \approx 350 \mu\text{m}$ ; uniform) side of the channel belt (Fig. 7). This exceeds scales and degrees of variations expected and attributable to erosion and deposition by small-scale bed forms such as subaqueous dunes (Miall, 1985; Van de Lageweg *et al.*, 2016). Cross-section B is located in the downstream part of Meander 2. The shift in lower bar deposits  $D_{50}$  characteristics appears not to be attributable to changes in local bank substrate conditions with translation of the meander. Instead, this can be explained by a change in the grain size of the material that was received from consecutive meanders upstream due to cut bank erosion and bed reworking in those locations. At first, this was mainly finer-grained material because the newly initiated channel predominantly mobilized fine-grained shallower substrate source material (Fig. 1: cover-sands), known to be fine-grained and homogenous ( $D_{50} \approx 200 \mu\text{m}$ , well-sorted; e.g. Winkels *et al.*, 2021). With proceeding meander translation, the bed sediment of these upstream meanders coarsened (in downstream and upstream subparts alike). The longer the river was established, the more it also entrained coarser substrate material eroded from below the cover-sands (Fig. 1: Late Pleistocene fluvial deposits). Early cover-sand admixtures thus would be gradually replaced in the overall grain-size signal in younger phases, progressively resulting in increased  $D_{50}$  variability. This is best seen in the relatively younger lower point-bar complexes in the north of the section within cross-section B.

Likewise, the lower bar deposits of Meander 5 in cross-section A comprise substrate material eroded and reworked by Meander 4 just upstream, which in addition to reworking Pleistocene cover-sand and buried coarse fluvial sand, also reworked Holocene fluvial sands from a precursor *Willeskop* channel-belt (Figs 6 and 10), which was fairly constant, resulting in the uniform properties of lower bar deposits observed in cross-section A.

The here described effect of local reworking and entrainment of substrate sands on the eventual grain-size of the StvCB point bars typically may occur in highstand coastal plain deltaic settings such as that of the Rhine-Meuse delta, where the Late Pleistocene (valley terracing) and Holocene (deltaic avulsion) fluvial history together made the delta plain substrate strongly heterolithic. In that setting, sandy substrate is predominantly encountered and reworked–entrained from a few metres below bankfull water depths, i.e. the substrate sands do not occur in the upper 1 to 3 m of the typical cut bank (Figs 6 to 8), which is different to the typical meander from a mixed-load river valley setting where meanders are relatively confined and laterally cut into sandy terraces. The deltaic setting thus not only provides for short-lived and spatially separated channel belts, but also provides a setting that is more diverse in uptake of local material, resulting in compositional heterogeneity (i.e.  $D_{50}$  variability).

The *upper bar deposits* in cross-section B seem to be less sensitive to changes in substrate uptake and/or upstream sediment supply. Still, a cluster of boreholes with well-developed CU trends in median grain-size is present that contrasts with the more common secondary-flow explained by FU trends (see above). Local, apparently systematic occurrence of CU trends within meander-belt deposits has been identified in multiple meandering systems elsewhere (e.g. McGowen & Garner, 1970; Lunt *et al.*, 2004; Pyrc & Ashmore, 2005; Wu *et al.*, 2015; Słowiak, 2016). Flow fields in meandering channels (from pool to downstream bar) may explain segregation of relatively coarse sediments in the topographically higher upstream and relatively finer sediment in downstream parts of a bend (Dietrich *et al.*, 1979; Bridge & Jarvis, 1982; Willis & Sech, 2019). Also in the StvCB the location where CU is observed in cross-section B, is at a relatively high and upstream part in Meander 3. In contrast, cross-section A which runs across the downstream end of a point bar, lacks any CU patches and shows FU trends in all boreholes. This supports to attribute the locally observed CUs sequences to past flow fields.

### Spatially resolved patterns of locally coarser deposits

Mapping  $D_{50}$  of the very top of the point bar complex reveals further coarse patches also between the main transects (Fig. 9). In other



meandering systems such phenomena often likely represent chute channel-bar deposits (e.g. McGowen & Garner, 1970; Van den Berg & Middelkoop, 2007; Ghinassi, 2011). Where flood-water flow paths cross older point bar complexes, causing local erosion of the original upper point bar, deposition of relatively coarser bed load sediments can occur. Cross-correlation between these coarse patches (Fig. 9) and reconstructed meander evolution (Fig. 10) reveals the superficial coarser patches to occur both in central and in downstream parts of the point bar. The pathways are influenced by the general orientation of the channel belt, which varies considerably along the investigated section of the StvCB, and can explain the variations in location, shapes and degree of relative coarseness seen in Fig. 9.

Importantly, relatively coarse patches are also found in the zone regarded to represent sandy abandoned channel fill (Fig. 9), meaning that the pattern cannot solely be explained as a product of active-stage chuting. The shallow occurrence of the coarse-grained patches in the abandoned channel zone, suggests that flood waters made occasional use of the abandoning channel depression, and entrained and reworked uppermost

point bar deposits residing from the active stage. Being able to identify this separately from the chuting process, supports our conceptual separation of these two architectural elements.

The key issue here is that the spatially resolved superficial coarse patches, as logged in the upper 50 cm of the sand body (this section, Fig. 9), should be regarded separately from the local CU trends identified over the upper 3 to 4 m in the topographically higher upstream part of Meander 3 in transect B (*Grain-size variability in lower and upper point bar deposits* section, Fig. 7). Interpretation of the depositional origin of coarsening-upward deposits within deltaic point bar deposits should therefore be met with caution, especially in the absence of planform reconstructions.

**Grain sizes in concave accretion zones**

Sediments within concave accretion zones reconstructed for the StvCB deviate markedly from the bulk of the boreholes within the convex point bar zones. The sediments within the concave parts of the StvCB point bars are remarkably finer than the coarser sandy material in the convex parts of the point bars (Fig. 11).

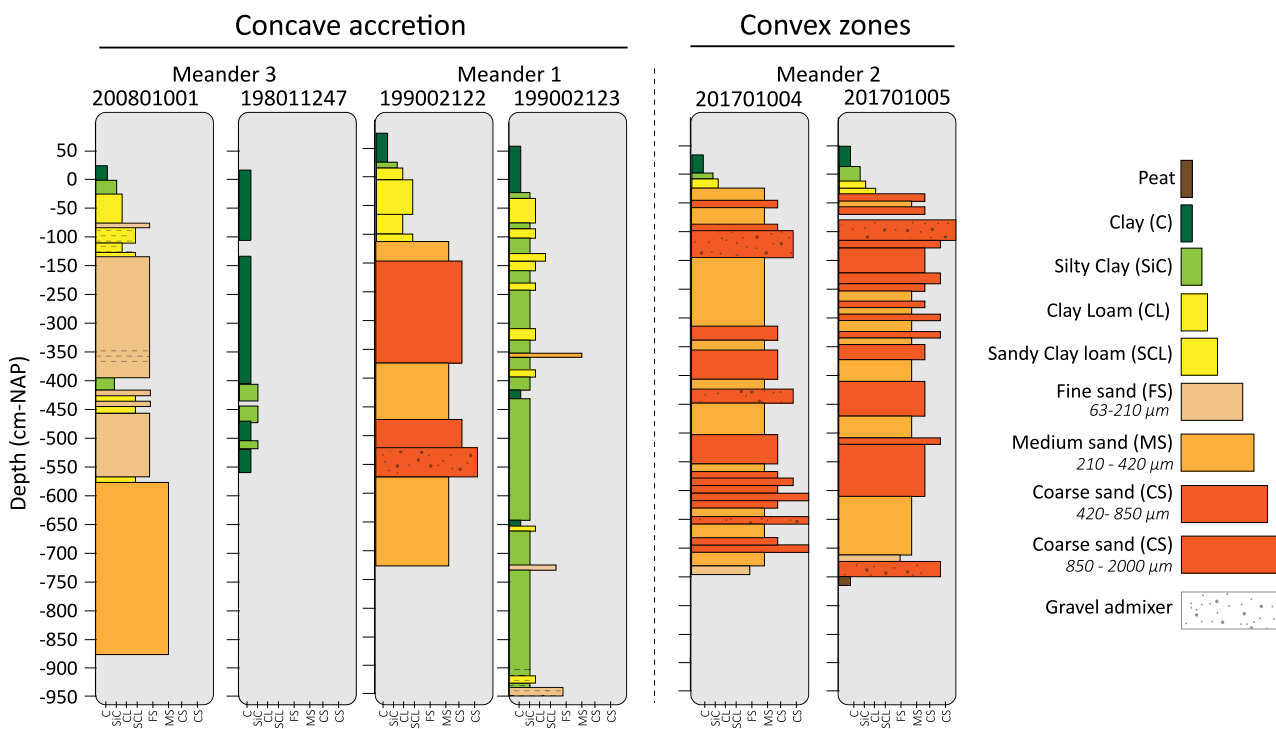


**Fig. 11.** Deep boreholes showing the sedimentary sequence within both concave accretion and convex zones. Locations of individual boreholes are shown in Fig. 10.

This makes identification of the concave zones important for hydrological and/or reservoir geological characterization of meandering river deposits (e.g. Smith *et al.*, 2009; Yan *et al.*, 2017; Durkin *et al.*, 2020). In the Rhine-Meuse delta, fine-clastic residual channel fill areas have received some explicit mapping attention (Berendsen, 1982; Pierik *et al.*, 2017), but fine-clastic pockets of other origin are not generally incorporated in channel belt mapping (Cohen *et al.*, 2012). Within specialist sedimentological studies, fine-clastic pockets interpreted as concave accretion zones have been identified in transects (e.g. Makaske & Weerts, 2005), but in regional mappings the non-sand profile types have typically been interpreted as other architectural elements (for example, crevasse; residual channel; natural levée deposits), without awareness of fine-grained concave accretion zones as an alternative. If full planform reconstructions are to become part of the geological-geomorphological mapping of channel belts in the Rhine-Meuse delta, such concave accretion zones can be better interpreted. The idea that fine-grained pockets marking concave accretion zones are often associated with meander migration through translation (Smith *et al.*, 2009, 2011; Sylvester *et al.*, 2021), may be guiding in such upgraded channel belt mappings containing planform-reconstructed meander evolution.

### Spatial reach of abandonment overprint

The avulsive nature of the meander belts leaves a distinct abandonment overprint in the youngest part of the sand body. Where an earlier study (Toonen *et al.*, 2012) contrasted the sedimentological build-up following avulsive channel abandonment (plugging, shallowing, narrowing; residual channel of multiple meanders length) with that of meander cut-off and oxbow formation (at the scale of single meanders), this study (*Planform architecture* section) emphasized the contrast between abandonment stage lithologies and main activity lithologies in the same system.

Where the StvCB sand body has minimum planform width, one-third of it is regarded as abandonment stage width, measured at the top of the sand body. Where meandering was translational and rotational and the StvCB sand body is wider (*Channel-belt structure* and *Meander evolution* sections), this fraction drops to a quarter to a fifth, such as between Meander 3 and Meander 4. At greater depth the channel width reduces (following the transverse bed

slope – Eq. 1, Table 1), and hence from a volumetric perspective roughly between one-sixth and one-tenth of the sand body sand would be trapped during the abandonment stage for the StvCB case (system activity:  $800 \pm 150$  years; *Stuivenberg channel belt* section). In longer-lived channel belt systems, the relative proportion is expected to be smaller due to the overall greater dimension of the systems, and quantification should also make a decision if localized meander cut-off oxbow plug bars (the contrast made in Toonen *et al.*, 2012) is reckoned to be part of active stage (because of chronology) or abandonment stage (because both are sandy channel fill). The latter also holds for meander belts within valley settings, where restriction of fluvial activity inhibits the frequent repositioning of fluvial systems. The research thus suggests that over 15 to 20% of the channel-belt surface area (i.e. top-of-sand) of typical Rhine-Meuse delta channel belts can be reckoned to be formed as part of the channel abandonment process, whereas roughly 75 to 80% reflects the upper point bar to levée facies transitions from the active stage. The *ca* 5% remaining would then be an area with fine-grained residual-channel and oxbow lake infill. This distinction in channel belt sandy facies is considered important for accurate hydrological characterization of meander belt deposits. The abandonment stage upper sands appear to have a higher percentage of admixture of silt-sized grains (*Supinfo S2*) that regular point bar deposits have not, which would decrease their hydraulic conductivity. Experimental ERT geophysical measurements (Olalla *et al.*, 2021, their fig. 6) return relatively lower resistivity values in this part of cross-section B (their BH2 is 2017 01 002 herein), which supports the deviating sedimentary characteristics of these sands.

### Lifespan of the channel belt

Various meander-belt planform and architecture studies have pointed out that reworking dynamics of meanders are governed by the erodibility of the local substrate, as well as that of deposits self-created by the system (e.g. Ferguson, 1987; Berendsen & Stouthamer, 2001; Makaske & Weerts, 2005; Smith *et al.*, 2009; Van de Lageweg *et al.*, 2014; Candel *et al.*, 2020). Looking at the StvCB, it is the short-lived nature of the system that has greatly reduced the complexity of its internal sedimentary architecture. There have been no meander cut-offs in the StvCB system

over the *ca* 800 years that it was active, before a new upstream avulsion made it abandon and internal reworking of inherent fluvial deposits is limited. This led to clear differences in sedimentary architecture which can be linked to meander evolution, without complicating factors such as continued reworking and neck and chute cut-off. Because abandonment stage deposits were separately treated, the authors could begin to quantify the part of sandy deposits attributable to that stage (10 to 14%; from *ca* 150 ± 100 years towards the end of activity) versus those of previous time (86 to 90%; from *ca* 650 ± 100 years). Proportionally, the active stage thus covers a dominant area of the meander belt, but in these short-lived systems the contribution of these abandonment stage sands appears significant.

If these results are upscaled for the Rhine-Meuse delta at large, regional variability in channel belt architecture and meander dynamics would be expected based on geologically understood variations in substrate configuration, and network-structure imposed and variations in duration of channel activity (e.g. Weerts, 1996; Berendsen & Stouthamer, 2000; Stouthamer *et al.*, 2011; Winkels *et al.*, 2021). The upper delta segment, for example, where floodplain width is narrower, has larger sized and longer-lived trunk channels mainly. Local mapping studies of various meander-belt deposits in this region revealed complicated architectures (Hesselink *et al.*, 2003; Kleinhans *et al.*, 2011), with abundant evidence for repeated cut-off and excessive self-reworking (and pre-deltaic meander belt and terrace gravel reworking, and bifurcation dynamic complexities). The floodplain widening that occurs with the transition to the lower delta segment, is associated with a much greater number (>20) of distributary channel belts, most of which are considerably smaller and short-lived, originating from partial avulsions predominantly (Stouthamer & Berendsen, 2000; Gouw, 2008; Stouthamer *et al.*, 2011; Winkels *et al.*, 2021). Typical duration for these short-lived deltaic branches is between 800 and 1200 years (Stouthamer & Berendsen, 2001, their Fig. 5). A few larger channel belts also exist, that are the 'trunk system' in traversing the lower delta which were active for 2000 to 5000 years (Stouthamer & Berendsen, 2001; Stouthamer *et al.*, 2011). It is the short-lived deltaic branches that, from an internal architectural-sedimentological perspective, are likely comparable to the StvCB.

## CONCLUSION

The planform approach described here towards explaining sedimentary architecture of the Stuivenberg channel belt (StvCB) revealed that systematic and spatially identifiable differences in sediment grain size occur within a single channel belt, which can be attributed to: (i) channel migration pattern; (ii) deposition during active stage versus abandonment stage of the channel; (iii) substrate lithological composition and architecture; and (iv) relative age of the point bar.

Channel-belt deposits belonging to the Holocene StvCB can be architecturally subdivided into an 'active stage: convex point bar', 'active stage: concave accretion zone' and 'abandoned channel zone' (all on planform-reconstructed criteria). The sediment in these zones shows contrasting grain-size characteristics in terms of median grain size, variability and vertical trends.

Upper and lower point bar deposits differ by their grain-size characteristics, with lower bars characterized by highly varying median grain sizes with no vertical trend, and upper bar deposits generally showing a classical fining-upward (FU) trend. Exceptions to these general characteristics can be attributed to incoming supply of upstream sediment of different grain sizes, and to the meander dynamics when the point bar developed. Within deposits from the main activity stage there is a sharp contrast in lithology found within classic point bar and concave accretion zones. The deposits in the first are predominantly sandy, whereas in the latter they comprise locally fine-grained clastic and fine-grained sandy deposits.

Results from this study show that, during the abandonment stage of a channel, considerable amounts of sand are deposited. In this case area, the abandonment stage left sandy deposits over *ca* 25% of the mean channel-belt width, making up 12% of the total sand volume in the channel belt. The deposits are characterized by a clear FU sequence developed over greater depth and relatively fine-grained and uniformly sorted sands (higher silt percentages), when compared to those in the adjacent point bar complex formed during main activity stage.

Locally patches of coarse-grained material occur within the upper 0.5 m of point-bar sand, which represent chute bar deposits. Coarse-grained patches identified in the abandoned channel zone predominantly lie adjacent to or just downstream of coarse-grained patches in the point-bar complex. This implies that sand of local origin was entrained and reworked into

the abandoned channel and further supports our activity related subdivision.

The short-lived avulsive nature of the StvCB and similar deltaic meander belt systems plays an important role in storage of sandy sediments in the deltaic channel belts – and has overprints on the lithological and hydrological/reservoir geological characteristics. Distinguishing between abandonment versus main activity stage deposits, as well as reconstruction of migration patterns of individual meanders, are important aspects to take into account when looking at the sedimentary architecture of these typical short-lived deltaic systems. In addition, it forms an important basis to advocate that the *duration* of channel activity should be considered as a prime discriminator for explaining the sedimentological character of channel belt sand bodies in avulsive distributary systems, and for contrasting these distributaries to trunk branches within deltas and meander belts in valleys.

## ACKNOWLEDGEMENTS

This research is part of the ‘Piping in practice’ project, funded by the Dutch Science Foundation, NWO-TTW (project number: 14502). Grain-size analysis was performed at VU Amsterdam, we thank M. Hagen and Dr M.A. Prins for their advice. We thank Bart Makaske and Chenliang Wu for critically reviewing this paper, and Massimiliano Ghinassi for his constructive comments for improvement of the manuscript.

## AUTHOR CONTRIBUTIONS

TGW and KMC jointly conceived the research. TGW performed revisiting fieldwork, grain-size lab work, dataset analysis and digital mapping. ES and KMC executed and coordinated earlier StvCB field campaigns and legacy data curation. TGW drafted the paper which was then edited by all co-authors.

## DATA AVAILABILITY STATEMENT

Data available on request from the authors.

## REFERENCES

Actueel Hoogtebestand Nederland 2 (2010) Retrieved from Website: AHN1 5 meter ruw 1996-2003 (RWS) | Data overhead.

- Actueel Hoogtebestand Nederland 3 (2017) Retrieved from Website: Actueel Hoogtebestand Nederland 3 (AHN3) | Data overhead.
- Aigner, T., Heinz, J., Hornung, J. and Aspiron, U. (1999) A hierarchical process-approach to reservoir heterogeneity: examples from outcrop analogues. *Bull. Centre Recherches Elf Explorat Product*, **22**, 1–11.
- Allen, J.R.L. (1963) The classification of cross-stratified units. With notes on their origin. *Sedimentology*, **2**, 93–114.
- Allen, J.R.L. (1965) Upper old red sandstone (Farlovian) paleogeography in South Wales and the Welsh borderland. *J. Sed. Res.*, **35**, 167–195.
- Allen, J.R.L. (1970) A quantitative model of grain size and sedimentary structures in lateral deposits. *Geol. J.*, **7**, 129–146.
- Beets, D.J. and van der Spek, A.J.F. (2000) The Holocene evolution of the barrier and the back-barrier basins of Belgium and The Netherlands as a function of late Weichselian morphology, relative sea-level rise and sediment supply. *Netherlands J. Geosci.*, **79**, 3–16.
- Berendsen, H.J.A. (1982) De genese van het landschap in het zuiden van de provincie Utrecht: een fysisch-geografische studie. PhD Thesis. Utrecht University.
- Berendsen, H.J.A. and Stouthamer, E. (2000) Late Weichselian and Holocene palaeogeography of the Rhine–Meuse delta, The Netherlands. *Palaeogeogr. Palaeoclimatol. Palaeoecol.*, **161**, 311–335.
- Berendsen, H.J.A. and Stouthamer, E. (2001) *Palaeogeographic Development of the Rhine–Meuse Delta*, p. 268. Van Gorcum, Assen, The Netherlands.
- Berendsen, H.J.A., Cohen, K.M. and Stouthamer, E. (2007) The use of GIS in reconstructing the Holocene palaeogeography of the Rhine–Meuse delta, The Netherlands. *Int. J. Geograph. Inf. Sci.*, **21**, 589–602.
- Berendsen, H.J.A. and Volleberg, K.P. (2007) New prospects in geomorphological and geological mapping of the Rhine–Meuse Delta-application of detailed digital elevation maps based on laser altimetry. *Netherlands J. Geosci.*, **86**, 15–22.
- Blott, S.J. and Pye, K. (2001) GRADISTAT: a grain size distribution and statistics package for the analysis of unconsolidated sediments. *Earth Surf. Proc. Land.*, **26**, 1237–1248.
- Bridge, J.S. and Jarvis, J. (1982) The dynamics of a river bend: a study in flow and sedimentary processes. *Sedimentology*, **29**, 499–541.
- Bridge, J.S., Alexander, J., Collier, R.E.L.L., Gawthorpe, R.L. and Jarvis, J. (1995) Ground-penetrating radar and coring used to study the large-scale structure of point-bar deposits in three dimensions. *Sedimentology*, **42**, 839–852.
- Busschers, F.S., Weerts, H.J.T., Wallinga, J., Cleveringa, P., Kasse, C., De Wolf, H. and Cohen, K.M. (2005) Sedimentary architecture and optical dating of middle and late Pleistocene Rhine–Meuse deposits-fluvial response to climate change, sea-level fluctuation and glaciation. *Netherlands J. Geosci.*, **84**, 25–41.
- Busschers, F.S., Kasse, C., Van Balen, R.T., Vandenberghe, J., Cohen, K.M., Weerts, H.J.T., Wallinga, J., Johns, C., Cleveringa, P. and Bunnik, F.P. (2007) Late Pleistocene evolution of the Rhine–Meuse system in the southern North Sea basin: imprints of climate change, sea-level oscillation and glacio-isostasy. *Quatern. Sci. Rev.*, **26**, 3216–3248.
- Candel, J.H.J., Kleinhans, M.G., Makaske, B., Hoek, W.Z., Quik, C. and Wallinga, J. (2018) Late Holocene channel pattern change from laterally stable to meandering – a

- palaeohydrological reconstruction. *Earth Surface Dynam.*, **6**, 723–741.
- Candel, J.H., Makaske, B., Kijm, N., Kleinhans, M.G., Storms, J.E. and Wallinga, J.** (2020) Self-constraining of low-energy rivers explains low channel mobility and tortuous planforms. *Depositional Rec.*, **6**, 648–669.
- Carey, W.C.** (1969) Formation of flood plain lands. *J. Hydraulics Div.*, **95**, 981–994.
- Chavez Olalla, J., Winkels, T.G., Ngan-Tillard, D.J.M. and Heimovaara, T.J.** (2021) Geophysical tomography as a tool to estimate the geometry of soil layers: relevance for the reliability assessment of dikes. *Georisk Assessment Manage. Risk Eng. Syst. Geohazards*, 1–21.
- Cohen, K.M., Stouthamer, E. and Berendsen, H.J.A.** (2002) Fluvial deposits as a record for late quaternary neotectonic activity in the Rhine-Meuse delta, The Netherlands. *Netherlands J. Geosci.*, **81**, 389–405.
- Cohen, K.M., Stouthamer, E., Pierik, H.J., and Geurts, A.H.** (2012) Digital Basisbestand Paleogeografie van de Rijn-Maas Delta/Rhine-Meuse Delta Studies' Digital Basemap for Delta Evolution and Palaeogeography.
- Cohen, K.M., Berendsen, H.J.A., Staff LLG (Utrecht University),** (2017) Laaglandgenese boringendatabase Universiteit Utrecht. DANS. <https://doi.org/10.17026/dans-zcvknya>.
- Colombera, L., Mountney, N.P. and McCaffrey, W.D.** (2013) A quantitative approach to fluvial facies models: methods and example results. *Sedimentology*, **60**, 1526–1558.
- De Bakker, H. and Schelling, J.** (1966) Systeem van bodemclassificatie voor Nederland. De hogere niveaus. *Grondboor Hamer*, **20**, 229.
- De Haas, T., Pierik, H.J., Van der Spek, A., Cohen, K.M., Van Maanen, B. and Kleinhans, M.G.** (2018) Holocene evolution of tidal systems in The Netherlands: effects of rivers, coastal boundary conditions, eco-engineering species, inherited relief and human interference. *Earth-Sci. Rev.*, **177**, 139–163.
- Dietrich, W.E., Smith, J.D. and Dunne, T.** (1979) Flow and sediment transport in a sand bedded meander. *J. Geol.*, **87**, 305–315.
- Durkin, P.R., Boyd, R.L., Hubbard, S.M., Shultz, A.W. and Blum, M.D.** (2017) Three-dimensional reconstruction of meander-belt evolution, Cretaceous McMurray Formation, Alberta foreland basin, Canada. *J. Sediment. Res.*, **87**(10), 1075–1099.
- Durkin, P.R., Hubbard, S.M., Holbrook, J., Weleschuk, Z., Nesbit, P., Hugenholtz, C., Lyons, T. and Smith, D.G.** (2020) Recognizing the product of concave-bank sedimentary processes in fluvial meander-belt strata. *Sedimentology*, **67**, 2819–2849.
- Fenneman, N.M.** (1906) Floodplains produced without floods. *Bull. Am. Geograph. Soc. New York*, **38**, 89.
- Ferguson, R.I.** (1987) Hydraulic and sedimentary controls of channel pattern. In: *River Channels: Environments and Processes* (Ed. Richards, K.S.), pp. 129–158. Blackwell, Oxford.
- Fisk, H.N.** (1947) *Fine-Grained Alluvial Deposits and Their Effects on Mississippi River Activity*. Mississippi River Commission, Vicksburg, MS.
- Fontana, A., Mozzi, P. and Marchetti, M.** (2014) Alluvial fans and megafans along the southern side of the Alps. *Sed. Geol.*, **301**, 150–171.
- Fryirs, K.A., Wheaton, J.M. and Brierley, G.J.** (2016) An approach for measuring confinement and assessing the influence of valley setting on river forms and processes. *Earth Surf. Proc. Land.*, **41**, 701–710.
- Ghinassi, M.** (2011) Chute channels in the Holocene high-sinuosity river deposits of the Firenze plain, Tuscany, Italy. *Sedimentology*, **58**, 618–642.
- Gibling, M.R.** (2006) Width and thickness of fluvial channel bodies and valley fills in the geological record: a literature compilation and classification. *J. Sed. Res.*, **76**, 731–770.
- Gouw, M.J.P. and Berendsen, H.J.A.** (2007) Variability of channel-belt dimensions and the consequences for alluvial architecture: observations from the Holocene Rhine-Meuse Delta (The Netherlands) and lower Mississippi Valley (USA). *J. Sed. Res.*, **77**, 124–138.
- Gouw, M.J.P. and Erkens, G.** (2007) Architecture of the Holocene Rhine-Meuse delta (The Netherlands)—a result of changing external controls. *Netherlands J. Geosci.*, **86**, 23–54.
- Gouw, M.J.** (2008) Alluvial architecture of the Holocene Rhine-Meuse delta (The Netherlands). *Sedimentology*, **55**, 1487–1516.
- Hesselink, A.W., Weerts, H.J.T. and Berendsen, H.J.A.** (2003) Alluvial architecture of the human-influenced river Rhine, The Netherlands. *Sed. Geol.*, **161**, 229–248.
- Hickin, E.J.** (1979) Concave-bank benches on the Squamish River, British Columbia, Canada. *Can. J. Earth Sci.*, **16**, 200–203.
- Hickin, E.J.** (1986) Concave-bank benches in the floodplains of Muskwa and Fort Nelson rivers, British Columbia. *Can. Geograph.*, **30**, 111–122.
- Hijma, M.P. and Cohen, K.M.** (2010) Timing and magnitude of the sea-level jump prelude the 8200 yr event. *Geology*, **38**(3), 275–278.
- Hijma, M.P. and Cohen, K.M.** (2011) Holocene transgression of the Rhine river mouth area, The Netherlands/southern North Sea: palaeogeography and sequence stratigraphy. *Sedimentology*, **58**, 1453–1485.
- Hijma, M.P. and Cohen, K.M.** (2019) Holocene Sea-level database for the Rhine-Meuse Delta, The Netherlands: implications for the pre-8.2 ka sea-level jump. *Quatern. Sci. Rev.*, **214**, 68–86.
- Hobo, N.** (2015) *The Sedimentary Dynamics in Natural and Human-Influenced Delta Channel Belts*. PhD Thesis. Utrecht University.
- Ielpi, A. and Ghinassi, M.** (2014) Planform architecture, stratigraphic signature and morphodynamics of an exhumed Jurassic meander plain (Scalby formation, Yorkshire, UK). *Sedimentology*, **61**, 1923–1960.
- Jones, L.S., Schumm, S.A., Smith, N.D. and Rogers, J.** (1999) Causes of avulsion: an overview. *Fluvial Sedimentol.* **VI**, **28**, 171–178.
- Jordan, D.W. and Pryor, W.A.** (1992) Hierarchical levels of heterogeneity in a Mississippi river meander belt and application to reservoir systems. *Am. Assoc. Petrol. Geol. Bull.*, **76**, 1601–1624.
- Julien, P.Y. and Wargadalam, J.** (1995) Alluvial channel geometry: theory and applications. *J. Hydraul. Eng.*, **121**, 312–325.
- Kleinhans, M.G., Cohen, K.M., Hoekstra, J. and Ijmker, J.M.** (2011) Evolution of a bifurcation in a meandering river with adjustable channel widths, Rhine delta apex, The Netherlands. *Earth Surf. Proc. Land.*, **36**, 2011–2027.
- Kleinhans, M.G., Ferguson, R.I., Lane, S.N. and Hardy, R.J.** (2013) Splitting rivers at their seams: bifurcations and avulsion. *Earth Surf. Proc. Land.*, **38**, 47–61.

- Konert, M.** and **Vandenbergh, J.** (1997) Comparison of laser grain size analysis with pipette and sieve analysis: a solution for the underestimation of the clay fraction. *Sedimentology*, **44**, 523–535.
- Krumbein, W.C.** (1934) Size frequency distributions of sediments. *J. Sed. Res.*, **4**, 65–77.
- Labrecque, P.A., Jensen, J.L., Hubbard, S.M.** and **Nielsen, H.** (2011) Sedimentology and stratigraphic architecture of a point bar deposit, lower cretaceous McMurray formation, Alberta, Canada. *Bull. Can. Petrol. Geol.*, **59**, 147–171.
- Latrubesse, E.M.** (2015) Large rivers, megafans and other quaternary avulsive fluvial systems: a potential “who’s who” in the geological record. *Earth-Sci. Rev.*, **146**, 1–30.
- Leopold, L.B.** and **Wolman, M.G.** (1957) *River Channel Patterns: Braided, Meandering, and Straight*, p. 85. US Government Printing Office, Washington.
- Lewis, G.W.** and **Lewin, J.** (1983) Alluvial cutoffs in Wales and the borderlands. In: *Modern and Ancient Fluvial Systems* (Eds Collinson, J.D. and Lewin, J.), *SEPM Spec. Publ.*, **6**, 145–154. Wiley, Hoboken.
- Lunt, I.A., Bridge, J.S.** and **Tye, R.S.** (2004) A quantitative, three-dimensional depositional model of gravelly braided rivers. *Sedimentology*, **51**, 377–414.
- Macklin, M.G.** and **Lewin, J.** (2003) River sediments, great floods and centennial-scale Holocene climate change. *J. Quat. Sci.*, **18**, 101–105.
- Makaske, B.** (2001) Anastomosing rivers: a review of their classification, origin and sedimentary products. *Earth-Sci. Rev.*, **53**, 149–196.
- Makaske, B.** and **Weerts, H.J.** (2005) Muddy lateral accretion and low stream power in a sub-recent confined channel belt, Rhine-Meuse delta, central Netherlands. *Sedimentology*, **52**(3), 651–668.
- McGowen, J.H.** and **Garner, L.E.** (1970) Physiographic features and stratification types of coarse-grained point bars: modern and ancient examples. *Sedimentology*, **14**, 77–111.
- Miall, A.D.** (1985) Architectural-element analysis: a new method of facies analysis applied to fluvial deposits. *Earth-Sci. Rev.*, **22**, 261–308.
- Miall, A.D.** (1991) Stratigraphic sequences and their chronostratigraphic correlation. *J. Sed. Res.*, **61**, 497–505.
- Middelkoop, H.** and **Asselman, N.E.M.** (1998) Spatial variability of floodplain sedimentation at the event scale in the Rhine-Meuse Delta, The Netherlands. *Earth Surf. Proc. Land.*, **23**, 561–573.
- Morozova, G.S.** and **Smith, N.D.** (2000) Holocene avulsion styles and sedimentation patterns of the Saskatchewan River, Cumberland marshes, Canada. *Sed. Geol.*, **130**, 81–105.
- Nanson, G.C.** and **Croke, J.C.** (1992) A genetic classification of floodplains. *Geomorphology*, **4**, 459–486.
- Nanson, G.C.** and **Page, K.** (1983) Lateral accretion of fine-grained concave benches on meandering rivers. *Mod. Ancient Fluvial Syst.*, 133–143.
- Oele, E., Apon, W., Fischer, M.M., Hoogendoorn, R.** and **Mesdag, C.S.** (1983) Surveying The Netherlands: sampling techniques, maps and their application. *Geologie en Mijnbouw*, **62**, 355–372.
- Page, K.** and **Nanson, G.** (1982) Concave-bank benches and associated floodplain formation. *Earth Surf. Proc. Land.*, **7**, 529–543.
- Paterson, G.A.** and **Heslop, D.** (2015) New methods for unmixing sediment grain size data. *Geochem. Geophys. Geosyst.*, **16**, 4494–4506.
- Payenberg, T. H., Lang, S. C., and Wibowo, B.** (2003) Discriminating fluvial from deltaic channels—examples from Indonesia. *Proceedings, Indonesian petroleum association*, October 2003.
- Payenberg, T., Willis, B., Fowler, J., Lang, S.C., Powell, A., Marsh, T., Smith, P.** and **Vakarelov, B.** (2019) Morphometrics of channel belts from the Mungaroo formation, NWS, Australia. *Petrol. Explor. Soc. Australia Symposium*, **1**, 11.
- Peeters, J., Busschers, F.S., Stouthamer, E., Bosch, J.H.A., Van den Berg, M.W., Wallinga, J., Versendaal, A.J., Bunnik, F.P.** and **Middelkoop, H.** (2016) Sedimentary architecture and chronostratigraphy of a late quaternary incised-valley fill: a case study of the late middle and late Pleistocene Rhine system in The Netherlands. *Quatern. Sci. Rev.*, **131**, 211–236.
- Pierik, H.J., Stouthamer, E.** and **Cohen, K.M.** (2017) Natural levee evolution in the Rhine-Meuse delta, The Netherlands, during the first millennium CE. *Geomorphology*, **295**, 215–234.
- Pierik, H.J.** and **Cohen, K.M.** (2020) The use of geological, geomorphological and soil mapping products in palaeolandscape reconstructions for The Netherlands. *Netherlands J. Geosci.*, **99**, 1–20.
- Pyrce, R.S.** and **Ashmore, P.E.** (2005) Bedload path length and point bar development in gravel-bed river models. *Sedimentology*, **52**, 839–885.
- Russell, C.E.** (2017) prediction of sedimentary architecture and lithological heterogeneity in fluvial point-bar deposits. PhD thesis. University of Leeds.
- Russell, C.E., Mountney, N.P., Hodgson, D.M.** and **Colombera, L.** (2019) A novel approach for prediction of lithological heterogeneity in fluvial point-bar deposits from analysis of meander morphology and scroll-bar pattern. In: *Fluvial Meanders and Their Sedimentary Products in the Rock Record* (Eds Ghinassi, M., Colombera, L., Mountney, N.P., Reesink, A.J. and Bateman, M.), pp. 385–417. John Wiley & Sons Ltd, Hoboken.
- Saucier, R.T.** (1994) *Geomorphology and Quaternary Geologic History of the Lower Mississippi Valley*, p. 399. US Army Engineer Waterways Experiment Station, Vicksburg, Mississippi.
- Słowik, M.** (2016) Sedimentary record of point bar formation in laterally migrating anabranching and single-channel meandering rivers (The Obra Valley, Poland). *Zeitschrift für Geomorphologie*, **60**(3), 259–279.
- Smith, D.G., Hubbard, S.M., Leckie, D.A.** and **Fustic, M.** (2009) Counter point bar deposits: lithofacies and reservoir significance in the meandering modern Peace River and ancient McMurray formation, Alberta, Canada. *Sedimentology*, **56**, 1655–1669.
- Smith, D.G., Hubbard, S.M., Lavigne, J.R., Leckie, D.A.** and **Fustic, M.** (2011) Stratigraphy of counter point bars and eddy accretion deposits in low energy meander belts of the Peace-Athabasca Delta, northeast Alberta, Canada. In: *From River to Rock Record: The Preservation of Fluvial Sediments and Their Subsequent Interpretation*, pp. 143–152. SEPM (Society for Sedimentary Geology), Tulsa.
- Sridhar, A.** and **Patidar, A.** (2005) Ground penetrating radar studies of a point-bar in the Mahi River basin, Gujarat. *Curr. Sci.*, **89**, 183–189.
- Stouthamer, E.** and **Berendsen, H.J.A.** (2000) Factors controlling the Holocene avulsion history of the Rhine-

- Meuse delta (The Netherlands). *J. Sed. Res.*, **70**, 1051–1064.
- Stouthamer, E. and Berendsen, H.J.** (2001) Avulsion frequency, avulsion duration, and interval avulsion period of Holocene channel belts in the Rhine-Meuse delta, the Netherlands. *J. Sediment. Res.*, **71**(4), 589–598.
- Stouthamer, E., Cohen, K.M. and Gouw, M.J.P.** (2011) Avulsion and its implications for fluvial-deltaic architecture: Insights from the Holocene Rhine-Meuse delta. In: *From River to Rock Record: The Preservation of Fluvial Sediments and Their Subsequent Interpretation* (Eds Davidson, S.K., Leleu, S. and North, C.P.), pp. 215–232. Society for Sedimentary Geology (SEPM, Special Publication 97), Tulsa.
- Sylvester, Z., Durkin, P.R., Hubbard, S.M. and Mohrig, D.** (2021) Autogenic translation and counter point bar deposition in meandering rivers. *GSA Bull.*, **133**, 2439–2456.
- Toonen, W.H.J., Kleinhans, M.G. and Cohen, K.M.** (2012) Sedimentary architecture of abandoned channel fills. *Earth Surf. Proc. Land.*, **37**, 459–472.
- Törnqvist, T.E.** (1993) Holocene alternation of meandering and anastomosing fluvial systems in the Rhine-Meuse delta (Central Netherlands) controlled by sea-level rise and subsoil erodibility. *J. Sed. Res.*, **63**, 683–693.
- Törnqvist, T.E.** (1994) Middle and late Holocene avulsion history of the river Rhine (Rhine-Meuse delta, Netherlands). *Geology*, **22**, 711–714.
- Van Asselen, S.** (2011) The contribution of peat compaction to total basin subsidence: implications for the provision of accommodation space in organic-rich deltas. *Basin Res.*, **23**, 239–255.
- Van de Lageweg, W.I., van Dijk, W.M., Baar, A.W., Rutten, J. and Kleinhans, M.G.** (2014) Bank pull or bar push: what drives scroll-bar formation in meandering rivers? *Geology*, **42**, 319–322.
- Van de Lageweg, W.I., van Dijk, W.M., Box, D. and Kleinhans, M.G.** (2016) Archimetrics: a quantitative tool to predict three-dimensional meander belt sandbody heterogeneity. *Depositional Record*, **2**, 22–46.
- Van de Plassche, O.** (1982) Sea-Level Change and Water-Level Movements in The Netherlands during the Holocene. PhD Thesis. Vrije Universiteit Amsterdam.
- Van den Berg, J.H. and Middelkoop, H.** (2007) Scroll bar and chute bar development in meandering rivers. Two contrasting examples: the lower Volga (Russia) and the Allier (France). *International Symposium on River Sedimentation*, **5**, 282–300.
- Weerts, H.J.** (1996) Complex Confining Layers: Architecture and Hydraulic Properties of Holocene and Late Weichselian Deposits in the Fluvial Rhine-Meuse Delta, The Netherlands. PhD thesis. Utrecht University.
- Werritty, A., Paine, J.L., Macdonald, N., Rowan, J.S. and McEwen, L.J.** (2006) Use of multi-proxy flood records to improve estimates of flood risk: lower river Tay, Scotland. *Catena*, **66**, 107–119.
- Willis, B.J. and Sech, R.P.** (2019) Emergent facies patterns within fluvial channel belts. In: *Meandering Rivers and Their Depositional Record* (Eds Ghinassi, M., Mountney, N., Colombera, L. and Reesink, A.J.), pp. 509–542. John Wiley & Sons Ltd, Hoboken.
- Winkels, T.G., Cohen, K.M., Knaake, S.M., Middelkoop, H. and Stouthamer, E.** (2021) Geological framework for assessing variability in subsurface piping parameters underneath dikes in the Rhine-Meuse delta, The Netherlands. *Eng. Geol.*, **294**, 362.
- Woodyer, K.D., Taylor, G. and Crook, K.** (1979) Depositional processes along a very low-gradient, suspended-load stream: the Barwon River, New South Wales. *Sed. Geol.*, **22**, 97–120.
- Wu, C., Bhattacharya, J.P. and Ullah, M.S.** (2015) Paleohydrology and 3D facies architecture of ancient point bars, Ferron sandstone, Notom Delta, south-Central Utah, USA. *J. Sed. Res.*, **85**, 399–418.
- Yan, N., Mountney, N.P., Colombera, L. and Dorrell, R.M.** (2017) A 3D forward stratigraphic model of fluvial meander-bend evolution for prediction of point-bar lithofacies architecture. *Comput. Geosci.*, **105**, 65–80.

Manuscript received 26 April 2021; revision accepted 13 June 2022

## Supporting Information

Additional information may be found in the online version of this article:

**Appendix S1** Excel<sup>®</sup> with grain-size data obtained for: (i) new cores (*Laboratory analysis new samples* section) and visualized in cross-section B (Fig. 7) and (ii) selected archived cores (UU-LLG database) in cross-sections A, B and C (Figs 6–8).

**Appendix S2** File containing the locations and lithological borehole data of all shallow cross-sections used for the ridge swale morphology reconstruction of Stuivenberg (Fig. 5).